SEMMELWEIS EGYETEM

DOKTORI ISKOLA

Ph.D. értekezések

3476.

TIM AUSBÜTTEL

A gyógyszerészeti tudományok korszerű kutatási irányai

című program

Programvezető: Dr. Antal István, egyetemi tanár

Témavezető: Dr. Boldizsár Imre, egyetemi docens

CAFFEIC ACID-CONTAINING COMPOUNDS AND LIGNANS DERIVED FROM SPECIES OF THE GENERA *ANTHRISCUS, FORSYTHIA* AND *LINUM*

PhD thesis

Tim Ausbüttel

Semmelweis University

Doctoral College

Pharmaceutical Sciences and Health Technologies Division

Supervisor: Imre Boldizsár, Ph.D.

Official reviewers: Ágnes M. Móricz, Ph.D.,
Arash Mirzahosseini, Ph.D.

Head of the Complex Exam Committee: Éva Szökő, D.Sc.

Members of the Complex Exam Committee: Anna Sólyomváry, Ph.D.,
Nóra Gampe, Ph.D.

Budapest
2026

TABLE OF CONTENTS

LIST OF ABBREVIATIONS

ACN	Acetonitrile
AHP	Anhydropodorhizol
AN	Arylnaphthalene
APT	Angeloyl podophyllotoxin
AT	Aryltetralin
ATP	Adenosine triphosphate
Bald.	Antonio Baldacci (1867–1950)
BVC	Beginning of the vegetation cycle
CC_{50}	half maximal cytotoxic concentration
CCC	Caffeic acid-containing compounds
CID	Collision-induced dissociation
CI	Characteristic ion
CQA	Caffeoylquinic acid
CPhEG	Caffeoyl phenylethanoid glycoside
DAD	Diode array detector
DBL	Dibenzylbutyrolactone
Degen	Árpád von Degen (1866–1934)
DeMeYA	Desmethylyatein
DiMA	Dimethylmatairesinol
DPT	Deoxypodophyllotoxin
DW	Distilled water
DWt	Dry weight
EC_{50}	Half maximal effective concentration
EICs	Extracted ion chromatograms
ESI	Electrospray ionization
FA	Forsythoside A
FF	*Forsythiae fructus*
FH	Forsythoside H
FI	Forsythoside I
FS	Flowering stage
HCV	human cytomegalovirus

HIV	Human immunodeficiency virus
HNSCC	Head and neck squamous cell carcinoma
HP	Highly polar
HPLC	High-performance liquid chromatography
HR-MS	High-resolution mass spectra
HSV-1	Herpes simplex virus type 1
HSV-2	Herpes simplex virus type 2
IC_{50}	Half maximal inhibitory concentration
IDPFG	Inverse detection pulsed field gradient
KAP	Kaerophyllin
L.	Carl Linnaeus (1707–1778)
MDiCQA	Malonyl-dicaffeoylquinic acid
MS^1	Full mass spectrometry scan
MS^2	Tandem mass spectrometry scan
MTT	Methylthiazolyldiphenyl-tetrazolium bromide
NF-κB	Nuclear factor ‘kappa-light-chain-enhancer’ of activated B-cells
NMR	Nuclear magnetic resonance
nd	Not detected
PC	Prostate cancer
PhEG	Phenylethanoid glycoside
PR	Pressure-resistant
PRM	Parallel reaction monitoring
RABV	Rabies virus
RNA	Ribonucleic acid
ROS	Reactive oxygen species
RSD%	Relative standard deviation percentage
RSV	Respiratory syncytial virus
RWG	Resonant waveguide grating
SARS-CoV-2	Severe acute respiratory syndrome coronavirus type 2
TCM	Traditional Chinese Medicine
TFA	Trifluoroacetic acid
Thunb.	Carl Peter Thunberg (1743–1828)

tr	Trace amounts
(U)HPLC(-MS)	(Ultra) High performance liquid chromatography (-mass spectrometry)
UV	Ultraviolet
v/v	Volume per volume
Vahl.	Martin Vahl (1749–1804)
w/w	Weight per weight
WNV	West nile virus
VSV	Vesicular stomatitis virus
YA	Yatein
ZIKV	Zika virus

1 INTRODUCTION

Caffeic acid-containing compounds (CCCs), including caffeoyl phenylethanoid glycosides (CPhEGs) and caffeoylquinic acids (CQAs), as well as lignans, are specialized plant metabolites belonging to the broad class of phenolic compounds with notable pharmacological relevance (1,2). CCCs and lignans are biosynthetically related, as caffeic acid serves as a key precursor in the formation of both metabolite groups: it is incorporated as a structural moiety in CCCs and acts as an intermediate in the biosynthesis of phenylpropanoid (C6C3) units that subsequently dimerize to form lignans (3,4).

Although CCCs and lignans differ in their chemical structures and biological functions, they frequently co-occur in numerous plant genera, including *Anthriscus*, *Forsythia*, and *Linum*, where they contribute to the medicinal properties of these taxa (5–7). Structurally, CPhEGs consist of a centrally positioned *β-D*-glucose core, whose hydroxyl groups are substituted with hydroxytyrosol, various saccharide residues, and one or more caffeic acid unit (1,8). In contrast, CQAs are characterized by a quinic acid core esterified with different organic acids, most commonly one or more caffeic acid moieties and, in some cases, malonic acid groups (2).

Lignans share a common structural motif based on the dimerization of two phenylpropanoid (C6C3) units derived from caffeic acid during biosynthesis. Owing to variations in the degree of side-chain oxidation, substitution patterns on the aromatic rings, and the presence or absence of unsaturation at specific carbon–carbon bonds, lignans display remarkable structural diversity. This diversity gives rise to several pharmacologically important subclasses, including aryltetralin (AT), dibenzylbutyrolactone (DBL), and arylnaphthalene (AN) lignans (3,9).

Plant species belonging to the genera *Anthriscus* and *Forsythia* have a long-standing history of use in traditional herbal medicine. However, only a limited range of plant organs has been employed for medicinal purposes and subjected to phytochemical investigation. Consequently, the specialized metabolite composition of other organs and tissues of these species remains largely unexplored (10–12). CCCs and lignans previously identified from *Anthriscus*, *Forsythia*, and *Linum* species have demonstrated notable antiviral and antiproliferative activities (13–15), highlighting the potential of these plants as sources of additional, yet unidentified bioactive compounds. Further investigation of

underexplored tissues may therefore lead to the discovery of novel metabolites with promising pharmacological properties.

1.1 Biosynthesis of phenylethanoid glycosides and caffeoylquinic acids

The biosynthesis of PhEGs, including their caffeoyl-containing representatives (CPhEGs), and CQAs originates from shikimic acid (2,16). Through the multistep shikimate pathway, shikimic acid is converted into the three metabolically essential aromatic amino acids *L*-phenylalanine, *L*-tryptophan, and *L*-tyrosine, which are synthesized from phosphoenolpyruvate and erythrose-4-phosphate (4). Among these, *L*-phenylalanine and *L*-tyrosine serve as key precursors for CPhEG biosynthesis. These amino acids are subsequently converted into CPhEGs through a series of enzymatic reactions within plant specialized metabolism, several of which remain incompletely characterized. A putative biosynthetic pathway for CPhEGs has been proposed by Alipieva and colleagues (17). During CQA formation, caffeic acid, biosynthesized from phenylalanine, can be coupled to quinic acid, an intermediate of the shikimate pathway (2).

1.2 Biosynthesis of lignans

The biosynthetic pathways of lignans and CPhEGs, both derived from *L*-phenylalanine and *L*-tyrosine, converge up to the formation of caffeic acid. In lignan biosynthesis, caffeic acid is subsequently converted into ferulic acid via O-methylation catalyzed by caffeic acid O-methyltransferase (4,16). Ferulic acid is then reduced to coniferaldehyde by cinnamoyl-CoA reductase, followed by further reduction to coniferyl alcohol catalyzed by cinnamyl alcohol dehydrogenase (4).

The final and decisive step of lignan biosynthesis is the oxidative, stereospecific coupling of two coniferyl alcohol molecules. This reaction is mediated by peroxidases or laccases in conjunction with dirigent proteins, which control the regio- and stereoselectivity of radical coupling. These enzymes generate phenoxyl radicals that undergo 8–8′ coupling to yield pinoresinol, a key precursor of many lignans. Through sequential, stereospecific enzymatic reactions catalyzed by pinoresinol–lariciresinol reductase and secoisolariciresinol dehydrogenase, pinoresinol is converted first into secoisolariciresinol and subsequently into matairesinol, a representative of

dibenzylbutyrolactone (DBL) lignans (18). This biosynthetic route is conserved across multiple plant species, including those of the genera *Forsythia* and *Linum* (3,18).

Starting from matairesinol, aryltetralin (AT) lignans (e.g., podophyllotoxin) and arylnaphthalene (AN) lignans can also be produced (19).

1.3 Arylnaphthalene, aryltetralin, and dibenzylbutyrolactone lignans: structure and occurrence

Among lignans, AN, AT, and DBL subclasses have been identified in *Anthriscus*, *Forsythia*, and *Linum* species (9). As described above, all lignans share a common structural feature in which two phenylpropanoid (C6C3) units are linked through an 8–8′ carbon–carbon bond. Lignans belonging to the AT and AN subclasses are further characterized by an additional carbon–carbon linkage between the two C6C3 units, specifically between the C2 and C7′ positions. The principal structural distinction between AT and AN lignans lies in the degree of unsaturations: AN lignans possess double bonds at the C7–C8 and C7′–C8′ positions, whereas these bonds are saturated in AT lignans (9,20). Notably, many AT and AN lignans also contain a *γ*-butyrolactone moiety, resulting in core structural features that closely resemble those of DBL lignans (**Figure 1**) (20).

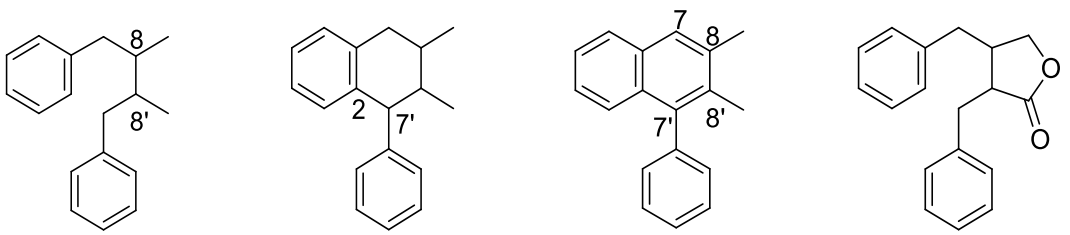

Figure 1. Base structure of lignans (A) belonging to aryltetralin (B), arylnaphthalene (C), and dibenzylbutyrolactone (D) groups (adapted from 9, 19, and 20).

1.3.1 Occurrence of aryltetralin and dibenzylbutyrolactone lignans

Several *γ*-butyrolactone ring-containing AT and DBL lignans have been identified in a variety of plant species (**Figure 2**). In the dried roots of *Anthriscus sylvestris* (L.) Hoffm. (cow parsley, Apiaceae), deoxypodophyllotoxin (**DPT**; 1.75 mg/g), angeloyl

podophyllotoxin (**APT**; 0.25 mg/g), anhydropodorhizol (**AHP**; 0.10 mg/g), yatein (**YA**; 1.1–18.5 mg/g), and dimethylmatairesinol (**DiMA**; 0.1–5.2 mg/g) have been quantified (11).

DPT has also been reported from the rhizomes of *Podophyllum peltatum* (mayapple) and *Sinopodophyllum hexandrum* (Himalayan mayapple) (21). **APT** was originally isolated from the roots of *A. sylvestris* (22), whereas **AHP** has additionally been identified in *S. hexandrum* (23). **YA** has been detected in *Juniperus chinensis*, *Bursera simaruba*, and *Hernandia nymphaeifolia* (3). Its dimethyl derivative, desmethylyatein (**DeMeYA**), has been reported in *P. peltatum*, where it functions as an intermediate in lignan biosynthesis (24). In addition, the DBL lignan kaerophyllin (**KA**) has been identified in the roots of *Chaerophyllum maculatum* (Apiaceae) (25).

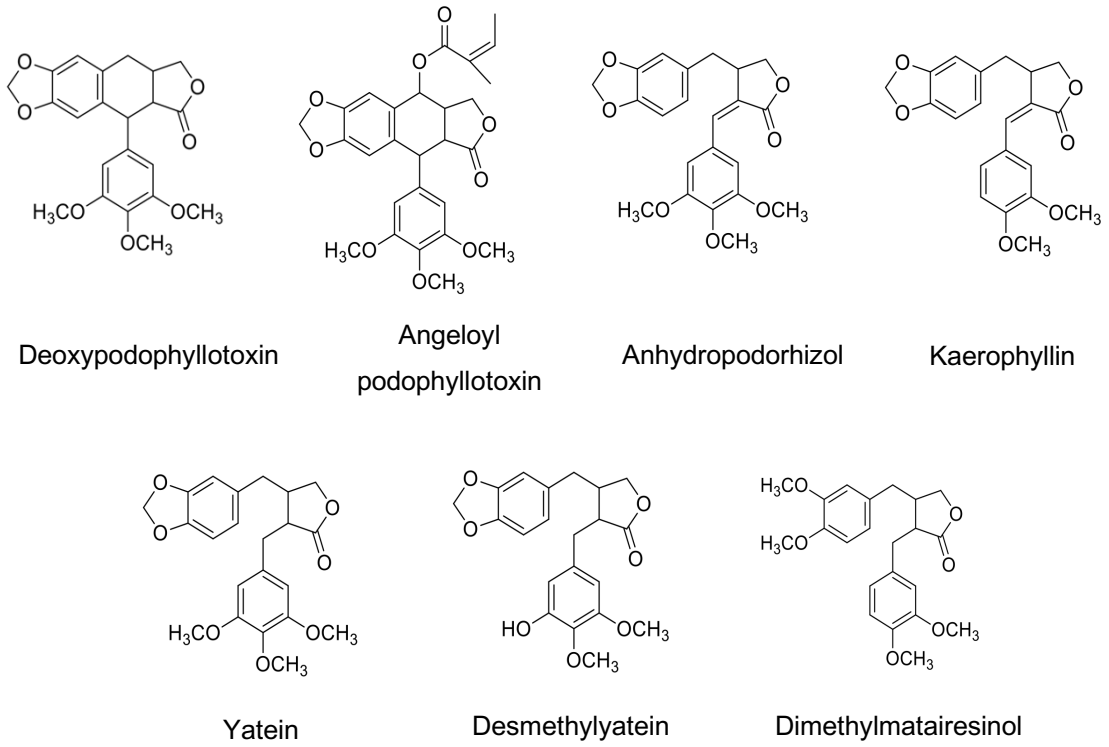

Figure 2. Representatives of aryltetralin and dibenzylbutyrolactone lignans (adapted from 21–25).

1.3.1 Occurrence of arylnaphthalene lignans

Within the genus *Linum*, AN lignans such as justicidin B and diphyllin are characteristic specialized metabolites and have been quantified in several *in vitro* culture

systems (**Figure 3**). Hairy root cultures of *L. corymbulosum* accumulated up to 40 mg/g dry weight (DWt) of justicidin B, whereas concentrations of 16.9 mg/g DWt and 10.8 mg/g DWt were reported for *L. austriacum* and *L. leonii*, respectively (26,27). In root cultures of *L. alpinum* and *L. austriacum*, justicidin B contents of 7.2 mg/g DWt and 5.3 mg/g DWt, respectively, were determined (28). Moreover, cell suspension cultures of *L. perenne* have been shown to accumulate justicidin B as a major component, further highlighting their potential as reliable sources of AN lignans (29). Diphyllin has also been identified in several *Linum* species; however, quantitative data are less extensive and typically indicate lower accumulation levels compared with justicidin B (14,30). Beyond the genus *Linum*, justicidin B has been reported in *Justicia procumbens* (Acanthaceae), *Phyllanthus* spp. (Euphorbiaceae), and *Haplophyllum* spp. (Rutaceae) (20,31). Diphyllin has likewise been identified in *Justicia procumbens*, *Haplophyllum sieversii* (Rutaceae), and *Cleistanthus collinus* (Euphorbiaceae) (20,32). In these taxa, however, the occurrence of these compounds is generally documented qualitatively, and reliable quantitative data are scarce. This limitation underscores the biotechnological advantage of *Linum in vitro* cultures as reproducible and high-yield sources of arylnaphthalene lignans (20).

However, to date, no data are available regarding the AN lignan composition of rhizomes and roots of *L. austriacum* and *L. perenne* grown outdoors.

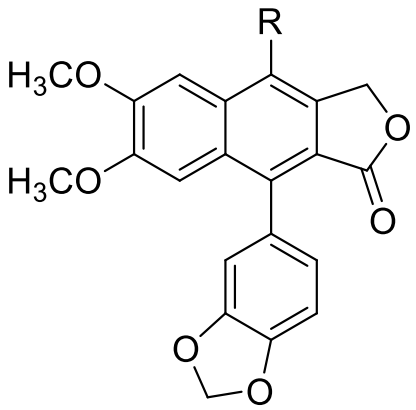

Figure 3. Structure of the arylnaphthalene lignans diphyllin (**R**=**OH**) and justicidin B (**R**=**H**) (adapted from 14 and 30).

1.4 Caffeoyl phenylethanoid glycosides: structure and occurrence

The CPhEG forsythoside A (**FA**) consists of a centrally positioned *β*-D-glucose that is linked at its C1, C4, and C6 hydroxyl groups to hydroxytyrosol, caffeic acid, and *α*-L-rhamnose units, respectively. Isomers of FA are also known, such as forsythoside H (**FH**) and forsythoside I (**FI**), whose caffeoyl units are linked at C2 and C3 positions, respectively (**Figure 4**) (33).

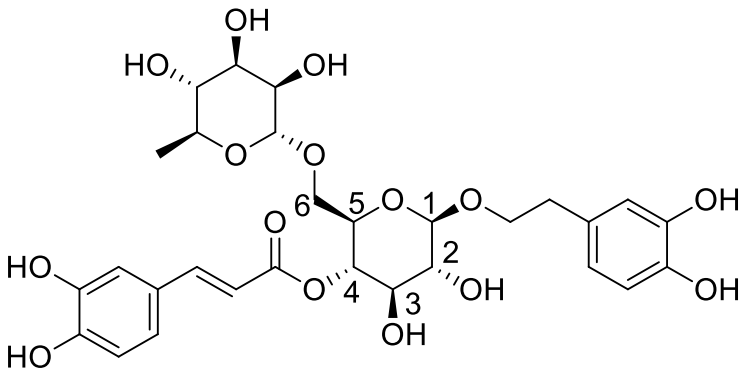

Figure 4. Chemical structure of the caffeoyl phenylethanoid glycoside forsythoside A (adapted from 33).

FA is a major constituent of the fruits, leaves, and bark of the genus *Forsythia* (34), with particularly high levels found in tea infusions prepared from the leaves of *F. suspensa* (35). The fruits of *F. suspensa* contain **FA** at reported levels ranging from 2.57 to 47.17 mg/g DWt, depending on the stage of development and plant organ (36). In addition to *Forsythia*, **FA** has been reported at lower levels in other plant families, including Plantaginaceae (*Isoplexis chalcantha*, 4 mg/g DWt) (37), Orobanchaceae (*Rehmannia glutinosa* callus cultures, 0.33 mg/g DWt) (38), and Calceolariaceae (*Calceolaria biflora*, 0.5 mg/g DWt) (39).

Studies on *F. suspensa* have shown that **FA** accumulates mainly in young, green fruits and seeds, traditionally known as *Qingqiao* in Traditional Chinese Medicine (TCM). However, its concentration decreases as the fruit ripens (33,36). Additionally, **FA** has been identified as the major CPhEG in the leaves of *Forsythia* species collected in Japan, with a reported content of 12.58 mg/g DWt (40).

FA, **FI**, and **FH** produce identical fragment ions in MS/MS analysis, and no established method currently distinguishes these three isomers based on their fragment ion profiles (41). The two isomers, **FH** and **FI**, were determined as minor metabolites present exclusively in the ripe, whole fruit of *F. suspensa* (36,42).

1.5 Caffeoylquinic acids: structure and occurrence

Caffeoylquinic acids (CQAs), including malonyl-1,4-*O*-dicaffeoylquinic acid, malonyl-1,5-*O*-dicaffeoylquinic acid, and malonyl-4,5-*O*-dicaffeoylquinic acid, were tentatively identified in the aerial parts of *A. cerefolium* using HPLC-HR-MS/MS (43). These compounds are characterized by a quinic acid core (1,3,4,5-tetrahydroxycyclohexanecarboxylic acid) esterified with two caffeic acid moieties and one malonic acid residue. Esterification of the hydroxyl groups at the **1**, **3**, **4**, and **5** positions of quinic acid with caffeic or malonic acid allows the formation of up to twelve regioisomeric MDiCQAs (**Figure 5**). In addition, the presence of chiral carbon atoms bearing hydroxyl groups enables epimerization of the quinic acid core, giving rise to further stereoisomeric MDiCQAs (2,44). This extensive regio- and stereochemical diversity presents a substantial challenge for the unambiguous structural identification of these compounds.

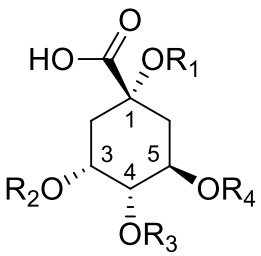

R_1	R_2	R_3	R_4
-caffeoyl	-malonyl	-H	-caffeoyl
-malonyl	-caffeoyl	-H	-caffeoyl
-caffeoyl	-H	-malonyl	-caffeoyl

Figure 5. Chemical structure of the tentatively identified malonyl-dicaffeoylquinic acids (adapted from 2, 43, and 44).

1.6 Genus *Forsythia*: description and medicinal significance

The genus *Forsythia* (family Oleaceae) comprises approximately 10 species native to eastern Asia, with a single exception: *F. europaea* Degen & Bald., which is indigenous to southeastern Europe. *Forsythia* species are deciduous shrubs characterized by opposite

leaves and bright yellow flowers that bloom in early spring, prior to leaf emergence. When present, the fruit is a capsule that dehisces at maturity, releasing numerous seeds (**Figure 6A**) (45).

Two species, *F. suspensa* Vahl and *F. viridissima* Lindl., as well as their hybrid *F.* × *intermedia*, are widely cultivated as ornamental plants in temperate regions worldwide for their attractive floral displays.

The fruits and leaves of *F. suspensa* have been used for centuries in traditional East Asian medicine: the fruits as anti-inflammatory and diuretic agents, and the leaves as a medicinal tea for the treatment of colds (46). Furthermore, the fruits of *F. suspensa* are listed as an official herbal drug in the Chinese, Japanese, and Korean Pharmacopoeias (47).

1.6.1 Pharmacological activity of CPhEG-type forsythoside isomers FA, FH, and FI from *Forsythia*

The antiinflammatory activity of **FA** has been well documented (48), while the antioxidant properties of **FA**, **FH**, and **FI** (40,50), as well as the antibacterial effects of **FH** and **FI** (49,50), have also been confirmed. In addition, **FA** has demonstrated notable antiviral activity against influenza virus (51) and avian infectious bronchitis virus (52).

1.7 *Linum* plants: description and medicinal significance

The genus *Linum* (family Linaceae) comprises approximately 200 species of flowering plants distributed primarily across temperate and subtropical regions worldwide. Members of the genus are herbaceous annuals or perennials that typically reach heights of 30–100 cm. They are characterized by slender stems bearing narrow, lanceolate leaves arranged alternately along the stem. Two representatives of blue-flowered flax species, *Linum austriacum* L. and *Linum perenne* L., are closely related and morphologically similar but can be distinguished by the orientation of their mature fruit pedicels, which are deflexed in *L. austriacum* and erect in *L. perenne* (53,54). Both species are native to Eurasia; however, *L. perenne* is also widely cultivated worldwide as an ornamental plant (55,56). These perennial species develop a woody underground rhizome that gives rise to roots and aerial, flowering, leafy shoots (**Figure 6B**) (53). To

the best of our knowledge, these two *Linum* species have not been reported to have traditional or established uses in herbal medicine.

1.7.1 Pharmacological activity of arylnaphthalene lignans diphyllin and justicidin B from *Linum* spp.

1.7.1.1 Antiviral effects

Among AN lignans isolated from *Linum* species, diphyllin and justicidin B have attracted considerable pharmacological interest due to their pronounced antiviral and antiproliferative activities. Diphyllin has been shown to exert broad-spectrum *in vitro* antiviral effects against both RNA and DNA viruses by inhibiting vacuolar-type H^+-ATPase (V-ATPase)-mediated endosomal acidification, a process essential for viral entry (27,57). Štefánik *et al.* (27) demonstrated that diphyllin effectively inhibits several clinically relevant enveloped viruses, including tick-borne encephalitis virus, West Nile virus, Zika virus (ZIKV), Rift Valley fever virus, rabies virus, and herpes simplex virus type 1 (HSV-1). The compound exhibited low cytotoxicity across the tested mammalian cell lines and reduced viral titres by 2–4 $\log_{10}$ units, supporting a host-directed antiviral mechanism rather than a direct virucidal effect. In addition to V-ATPase inhibition, multiple host-directed mechanisms appear to contribute to its antiviral activity.

Justicidin B has likewise demonstrated potent antiviral activity. Ferraz *et al.* (58) reported that justicidin B markedly inhibits ZIKV replication in Vero cells, with treatment at 12.5 μM reducing viral RNA levels by approximately 99.9% compared with untreated controls. Cytotoxicity assessment using the MTT assay indicated minimal effects on uninfected Vero cells, yielding a CC_{50} value exceeding 100 μM and a selectivity index ($SI=CC_{50}/IC_{50}$) greater than 8. Together, these findings indicate that justicidin B is a highly effective and selective inhibitor of ZIKV replication.

1.7.1.2 Antiproliferative effects

Justicidin B exhibits pronounced cytotoxic and pro-apoptotic activity across a variety of tumor cell lines. It displays IC_{50} values of approximately 1 μM against human leukemia (LAMA-8) and breast cancer (MCF-7 and MDA-MB-231) cell lines (59,60). Sciandrone *et al.* (61) demonstrated that justicidin B suppresses cancer cell growth and survival primarily by inducing apoptosis. In HeLa cells, treatment with justicidin B

increased the ratio of the pro-apoptotic protein Bax to the anti-apoptotic protein Bcl-2 and activated caspase-3, indicating involvement of the intrinsic mitochondrial apoptotic pathway. Importantly, *in vivo* toxicity studies in mice (up to 50 mg/kg) and *Caenorhabditis elegans* (up to 100 µg/mL) revealed low systemic toxicity, suggesting that justicidin B preferentially targets tumor cells while being well tolerated by normal biological systems (61).

Diphyllin has likewise been explored for its anticancer potential. As discussed above, diphyllin inhibits vacuolar-type H^+-ATPase, leading to intracellular acidification and apoptosis. In head and neck squamous cell carcinoma cells (HNSCC), treatment with 5–10 µM diphyllin significantly reduced cell viability and induced caspase-dependent apoptotic cell death (62). A recent review further confirmed the antitumor activity of diphyllin across multiple human cancer models, identifying V-ATPase inhibition as its primary mechanism of action (63).

1.8 *Anthriscus* plants: description and medicinal significance

The genus *Anthriscus* (family Apiaceae) comprises 10–14 accepted species distributed across temperate Eurasia and parts of North and East Africa. This number varies among taxonomic treatments due to differing interpretations of closely related taxa and emerging molecular data clarifying relationships within the genus. Species are typically herbaceous annuals, biennials, or short-lived perennials characterized by thickened taproots, hollow, grooved stems, and finely divided, bipinnate to tripinnate leaves. Inflorescences are compound umbels bearing small white flowers, and the fruits are two-parted schizocarps with diagnostic surface features (**Figure 6C**) (64–66).

The traditional medicinal use of *A. sylvestris* includes preparations made from its aerial parts, such as the inflorescences. These have been used as tonics and diuretics, as well as in poultices for wound dressing (67). Extracts prepared from flowering umbels have demonstrated antioxidant, anti-inflammatory, and cytoprotective activities, primarily attributed to their high content of flavonoids, phenolic acids, and lignans (68,69). Recent *in vitro* studies have supportingly reported that inflorescence extracts reduce reactive oxygen species (ROS) and suppress inflammatory mediators in human fibroblast and macrophage cell lines. This supports the potential use of such extracts in dermatological and anti-inflammatory formulations (70,71). Earlier pharmacological

studies have also indicated that fractions derived from *A. sylvestris* inflorescence exhibit moderate cytotoxic and antimicrobial properties (15).

The leaves of *A. sylvestris* have been traditionally employed in European folk medicine, where young foliage was used either raw or cooked as a potherb and occasionally as a flavouring agent, and more explicitly as a diuretic tonic and remedy for headaches and general weakness (67,72). Ethnobotanical surveys have recorded the use of decoctions made from the aerial parts, including the leaves, to alleviate urinary retention, kidney discomfort and general fatigue in rural communities (67,73,74).

In traditional medicine, root preparations were used as infusions or decoctions to treat fever, cough, and urinary disorders, and were also applied externally as poultices to reduce inflammation, swelling, and pain (75). These traditional medicinal uses align with the later attributed antiproliferative and anti-inflammatory properties of lignans and lignan-rich extracts from *A. sylvestris* (71,15).

Only limited data exist on the aerial parts of *A. caucalis*, which have been analyzed for their essential oil composition, whereas no phytochemical or medicinal information is available for *A. nitida* (76).

A **B** **C**

Figure 6. General morphological characteristics of *Forsythia suspensa* (**A**), *Linum perenne* (**B**), and *Anthriscus sylvestris* (**C**) (author's own work).

1.8.1 Pharmacological activity of aryltetralin and dibenzylbutyrolactone lignans from genus *Anthriscus*

1.8.1.1 Antiviral activity of compounds

AT and DBL lignans isolated from *A. sylvestris*, particularly deoxypodophyllotoxin (**DPT**) and yatein (**YA**), exhibit notable broad-spectrum antiviral activities. **DPT** has been shown to inhibit HSV-1 replication in MRC-5 human fibroblast cells with an IC_{50} value of 0.15 μM, while displaying low cytotoxicity toward host cells (15,77). Comparable inhibitory activity was observed against HSV-2, indicating that these lignans interfere with viral replication processes (77).

In contrast, inhibitory activity of **YA** and its desmethyl derivative (**DeMeYA**) against either HSV-1 or vesicular stomatitis virus (VSV) was not reported in the cell-based assays described (78). Further studies on podophyllotoxin-type lignans structurally related to **DPT** and **YA** demonstrated inhibitory effects against human cytomegalovirus (HCV) and respiratory syncytial virus (RSV) *in vitro* (77,79). Moreover, kaerophyllin (**KAP**) has been identified as a promising antiviral candidate *in silico*, exhibiting strong docking affinities toward multiple ZIKV nonstructural proteins, including NS3 helicase and NS5 RNA-dependent RNA polymerase (80).

Collectively, these findings suggest that selected root-derived lignans from *A. sylvestris* exhibit antiviral activity *in vitro* and warrant further investigation as leads for the development of antiviral agents. **Table 1** summarizes the antiviral activities of these lignans reported in the literature. Antiviral activity has not been reported for the DBL lignans dimethylmatairesinol (**DiMeMAT**) and anhydropodorhizol (**AHP**), nor for the AT lignan angeloyl podophyllotoxin (**APT**), in the literature discussed here.

1.8.1.2 Antiproliferative activity of compounds

DPT exhibited pronounced antiproliferative and cytotoxic activity against a wide range of human cancer cell lines. In human gastric carcinoma SGC-7901 cells, **DPT** induced G_2/M cell-cycle arrest and apoptosis through activation of the mitochondrial pathway and downregulation of the anti-apoptotic protein Bcl-2 at low nanomolar concentrations (81). Comparable effects have been reported in prostate cancer DU-145 cells, where **DPT** promotes caspase-3-dependent apoptosis and inhibits cell proliferation at nanomolar concentrations (82). More recently, **DPT** has been shown to inhibit the

growth of non-small-cell lung cancer A549 cells by suppressing HIF-1α–mediated glycolysis, resulting in reduced tumour growth *in vivo* (83) (**Table 1**).

Table 1. A review of the literature on the antiproliferative and antiviral activities of lignans isolated from *A. sylvestris*.

Lignan	**antiproliferative**	**antiviral**
Desmethylyatein	P-388 cells IC_{50} 10 µg/mL (96)	no anti HSV activity (96) no anti VSV activity (96)
Dimethylmatairesinol	KKU-M 100 cells (97)	
Deoxypodophyllotoxin	KYSE 30 - IC_{50} 7,64 nM */ 450 IC_{50} - 8,10 nM *(ESCC cells via EGFR-inhibition (1)) *48 h (98) HeLa cervical carcinoma cells - loss of microtubule network at 0,25 µM (100) HL-60 cells - increase of caspase-3 activity + DNA fragmentation at 0,0001 µM (105) P-388 cells (lymphoid neoplasm) IC_{50} 0,0025 - 0,005 µg/mL (96)	HSV Itoh strain EC_{50} 0,004 µg/mL (101) HSV-1 replication EC_{50} 0,03 µM (102)
Yatein	P3X cells ind. 75 % cell death at 25 µg/mL (106) P-388 cells (lymphoid neoplasm) IC_{50} 0,025 µg/mL (96)	no anti HSV activity (96,101) no anti VSV activity (96)
Kaerophyllin	brine shrimp lethality test: ED_{50} 44 µg/mL (107)	*in silico:* exhibited an average docking score of −110.5 kJ/mol across the five investigated ZIKV non-structural proteins (80)
Anhydropodorhizol	Brine shrimp lethality test: ED_{50} 54 µg/mL (107)	
Angeloyl podophyllotoxin	HL-60 cells – increase of caspase-3 activity + DNA fragmentation at 0,001 µM (105)	

Furthermore, **DPT** acts as a potent microtubule-destabilizing agent (100). Despite its pronounced antiproliferative and pro-apoptotic effects, **DPT** exhibits considerably lower toxicity in normal cells, including human fibroblasts (MRC-5), endothelial cells (HUVEC), and liver cells (LO2) (81,83,84), suggesting a moderate degree of tumor selectivity. Nevertheless, the pronounced bioactivity of **DPT** underscores the need for

careful evaluation of its safety profile before therapeutic application can be considered. **YA** has demonstrated growth-inhibitory activity in human leukemia (HL-60), lung (A549), and breast (MCF-7) cancer cell lines. Mechanistic studies in A549 cells revealed that **YA** induces G_2/M cell-cycle arrest and apoptosis through microtubule destabilization (85). In contrast, **DeMeYA** and **DiMA** exhibited weaker cytotoxic effects in comparative assays (78). Additional data on the antiproliferative activity of *Anthriscus*-derived lignans are summarized in **Table 1**.

Collectively, these findings underscore the structure-dependent biological activity of *A. sylvestris* lignans and highlight the need for further pharmacological investigation of less-studied congeners.

1.8.2 Pharmacological activity of malonyl-dicaffeoylquinic acids

Since MDiCQAs have only been tentatively identified and not isolated, their biological activity has not yet been experimentally evaluated.

1.9 Concluding remarks on the literature survey

Based on the reviewed literature related to our research topic (1–109), the following conclusions can be drawn:

1) The isomeric CPhEGs forsythosides A, H, and I (**FA**, **FH**, **FI**) have been identified in the fruits of *Forsythia suspensa*, with **FA** as the dominant constituent and **FH** and **FI** occurring as minor compounds. Discrimination between these isomers by MS/MS has not been performed.

2) Given the known presence of AN lignans in *Linum* species, their occurrence in the underground organs (rhizomes and roots) of *L. austriacum* and *L. perenne*, which have not yet been investigated for these compounds, can be assumed.

3) Considering the frequent co-occurrence of lignans and caffeic acid-containing compounds (CCCs), e.g., CQAs, it can be hypothesized that CCCs are present in *Anthriscus sylvestris*, a species already known to contain lignans, and that CCCs and/or lignans occur in *A. caucalis* and *A. nitida* despite the absence of previous phytochemical reports.

4) Since many CCCs and lignans have demonstrated antiproliferative and antiviral activities, related compounds from *Anthriscus*, *Forsythia*, and *Linum* species also warrant investigation for identification, isolation, and bioactivity evaluation.

2 OBJECTIVES

The aims of our work were:

1) To analyze the MS fragment ion profiles of isomeric CPhEGs in order to identify diagnostic ions suitable for distinguishing between the isomeric compounds.

2) To determine the arylnaphthalene lignan composition in the underground organs (i.e., in roots and rhizomes) of *Linum austriacum* and *L. perenne*.

3) To follow arylnaphthalene lignan accumulation in the roots and rhizomes of *L. austriacum* and *L. perenne* during a full vegetation cycle of one year.

4) To develop acidic and enzymatic treatment procedures for arylnaphthalene lignan conversions, aiming to obtain structure-specific information and increase levels of minor compounds.

5) To define optimum tissues and treatment procedures, allowing for the isolation of high-purity arylnaphthalene lignans from *Linum* plants.

6) To determine the aryltetralin and dibenzylbutyrolactone lignan composition as well as the CQA profile and their accumulation in various organs of *A. caucalis*, *A. nitida,* and *A. sylvestris* during a full vegetation cycle of one year.

7) To identify optimal tissues with relatively high levels of selected compounds, facilitating their isolation.

8) To determine the *in vitro* cytostatic activities of isolated compounds against normal healthy cells (Vero E6) and various human cancer cell lines to assess their safety and potential for further drug development.

9) To evaluate the *in vitro* antiviral potential of the isolated arylnaphthalene lignans against the SARS-CoV-2 virus and on various human cancer cell lines, respectively.

3 MATERIAL AND METHODS

3.1 Plant material

3.1.1 Fruit samples of *Forsythia suspensa* Vahl (Oleaceae)

Samples were collected from the Botanical Garden of Szent István University (Budapest, Hungary, Villányi street 29–43): the unripe, green fruits in July of 2018. The collected samples were immediately lyophilized on the day of collection.

3.1.2 Underground organs of *Linum austriacum* L. and *Linum perenne* L. (Linaceae)

Samples, i.e., roots and rhizomes, were collected from different Hungarian locations four times during a full vegetation cycle of one year: in April, June, September, and December of 2020. At each sampling time, at least ten plants were collected. The roots and rhizomes of these plants were manually separated. These roots and rhizomes were pooled to prepare the rhizome and root samples. The collected samples were immediately lyophilized on the day of collection.

3.1.3 Samples of *Anthriscus caucalis* M. Bieb., *Anthriscus nitida* (Wahlenb.) Hazsl. and *Anthriscus sylvestris* (L.) Hoffm. (Apiaceae)

Samples were collected from different Hungarian locations at the beginning of the vegetation cycle (in January and February) and in the flowering stage (in April and May). At each sampling time, at least ten plants were collected. Organs were manually separated and pooled to prepare the root, leaf, and inflorescence samples. The collected samples were immediately lyophilized on the day of collection.

3.2 Extractions for analyses and isolations, performing various treatments for compound conversions

The solvents applied in the analyses, isolations, and various treatments, such as acetonitrile (ACN), distilled water (DW), formic acid (FAc), methanol, and trifluoroacetic acid (TFA) (Reanal, Hungary), were all of analytical reagent grade of the highest purity available.

3.2.1.1 Preparation of plant extracts

Lyophilized and pulverized plant tissues (100.0 mg) were extracted three times consecutively with 5 mL of methanol at 60 °C in 25 mL screw-capped vials for 30 min to prepare 15.0 mL stock solutions. These stock solutions were used after their dilution with methanol for HPLC-UV-HR-MS analyses.

3.2.2 *Linum* species: Extract preparation for analysis and isolation, and performing heat treatments and enzymatic conversions

3.2.2.1 Performing endogenous enzymatic treatment

Lyophilized and pulverized plant tissues (100.0 mg) were suspended in 2.0 mL of DW in 25 mL screw-capped vials. These suspensions were left for 30 min at room temperature, allowing for enzymatic conversions of compounds in an aqueous medium. Thereafter, the samples were lyophilized and extracted according to the protocol shown in the following section.

3.2.2.2 Preparation of plant extracts for analysis and isolation

Lyophilized and pulverized intact plant tissues (100.0 mg), as well as enzyme-treated and lyophilized tissues, were extracted three times consecutively with 5 mL of methanol at 60 °C in 25 mL pressure-resistant (PR) screw-capped vials for 30 min to prepare 15.0 mL stock solutions. These stock solutions were used for HPLC-UV-HR-MS analyses. Dried aliquots (5.0 mL) of the stock solutions prepared from the intact *L. austriacum* root and rhizome samples (collected in September and marked with collection number **A1**) were dissolved in 0.5 mL of methanol for the isolation of linadiacin A by preparative HPLC.

3.2.2.3 Performing acid treatments

3.2.2.3.1 Acid treatment optimization of isolated linadiacin A

0.774 mg of isolated linadiacin A (corresponding to 1.00 µmol) was dissolved in 1.0 mL 0.2 M TFA and 2 M TFA (in 5 mL PR screw-capped vials). These solutions were heated at 100 °C for 3, 10, and 30 min. The samples were dried using a vacuum evaporator (at 30–40 °C). The dried samples were analyzed after their dissolution in methanol by HPLC-UV-HR-MS.

3.2.2.3.2 Acid treatments of root and rhizome extracts

Dried aliquots (5.00 mL) of the stock solution prepared from the intact *L. austriacum* root sample (collected in September and marked with collection number **A1**) were dissolved in 1.0 mL of 2 M TFA (in 5 mL PR screw-capped vials). These solutions were heated at 100 °C for 3 min and 30 min. After heating, the samples were dried using a vacuum evaporator (at 30–40 °C). The dried samples were dissolved in 5.00 mL and 0.5 mL of methanol before the analyses and isolations, performed by HPLC-UV-HR-MS and preparative HPLC, respectively. The isolation of linadiacin B after the 3 min acid treatment and of diphyllin and justicidin B after the 30 min acid treatment was performed by preparative HPLC.

3.2.3 *Anthriscus* species: Preparation of extracts for analysis and isolation

Lyophilized and pulverized plant tissues (10.0 mg) were extracted with 3.0 mL of methanol at 60 °C for 30 minutes in 5 mL PR screw-capped vials. The extracts were centrifuged at 5,000 rpm using a standard laboratory centrifuge before HPLC-UV-HR-MS analysis. For compound isolation, pulverized plant tissues (2 g) were extracted thrice with 15 mL of methanol at 60 °C in PR screw-capped vials for 30 minutes each. The centrifuged supernatants were combined and dried using a standard laboratory rotary vacuum evaporator. The dried extracts were dissolved in 5 mL of methanol and centrifuged at 5000 rpm. After centrifugation, the supernatant was filtered using Minisart RC 15 syringe filters (0.2 µm pore diameter, Sartorius AG, Goettingen, Germany) before preparative HPLC separation.

3.3 Analytical and preparative HPLC separations

3.3.1 Instruments, eluents and general settings for analytical HPLC with UV and high-resolution Orbitrap mass spectrometric detections

A Dionex Ultimate 3000 UHPLC system (3000RS diode array detector (DAD), TCC-3000RS column thermostat, HPG-3400RS pump, SRD-3400 solvent rack degasser, WPS-3000TRS autosampler), hyphenated with an Orbitrap Q Exactive Focus Mass Spectrometer equipped with electrospray ionization (ESI) (Thermo Fischer Scientific, Waltham, MA, USA) was used for analysis. MS parameters were optimized automatically using the built-in software as follows: spray voltage, 2500 V (-); capillary

temperature 320 °C; sheath-, auxiliary-, and spare-gases (N2): 47.52, 11.25, and 2.25 arbitrary units, respectively. Full scan resolution: 70,000 in the scanning range of m/z 100–1000. MS/MS scan resolution: 35,000 in the scanning range of m/z 80–1000 m/z. Mobile phases: 0.1% (v/v) formic acid (A) and 8:2 ACN:0.1% (v/v) formic acid (B); injected volume: 1.0 µL–5 µL; DAD spectra were recorded between 250 and 600 nm.

3.3.2 Separations by analytical HPLC

3.3.2.1 *Forsythia suspensa*

Gradient: 0.0 min, 10% B; 4.0 min, 20% B (linear gradient); 8.0 min, 20% B (isocratic); 13.0 min, 70% B (linear gradient). Flow rate: 0.3 mL/min. Column: Kinetex XB-C18 column (50 × 3.0 mm; 1.7 µm) (Phenomenex, USA).

3.3.2.2 *Linum* species

Gradient: 0.0 min, 20% B; 24.0 min, 40% B (linear gradient); 30.0 min, 70% B (linear gradient); 31.0 min 70% B (isocratic). Flow rate: 0.3 mL/min. Column: Kinetex C18 column (75 × 3 mm; 2.6 µm) (Phenomenex, Torrance, CA, USA).

3.3.2.3 *Anthriscus* species

Gradient program 1: 0.0 min, 20% B; 15.0 min, 90% B (linear gradient); 18.0 min, 90% B (isocratic). Gradient program 2: 0.0 min, 15% B; 15.0 min, 50% B (linear gradient); 16.0 min, 90% B (linear gradient); 19.0 min, 90% B (isocratic). Flow rate: 0.4 mL/min. Column: Gemini NX-C18 column (150 × 3 mm; 3 µm) (Phenomenex, USA).

3.3.3 Preparative HPLC

3.3.3.1 Instruments

3.3.3.1.1 Preparative HPLC instrument for the isolation of compounds from *Linum* species, and that for the isolation of lignans from *Anthriscus* species

A Pharmacia LKB HPLC (Uppsala, Sweden) system (2248 pumps, VWM 2141 UV detector) was connected to a preparative HPLC. Column: Gemini NX-C18 (5 µm), 250 × 10 mm (Phenomenex, USA).

3.3.3.1.2 Preparative HPLC instruments for the isolation of malonyl-dicaffeoylquinic acids from *A. sylvestris*

A Dionex UltiMate 3000 HPLC System (VWD-3400RS photometer, HPG-3200BX pump, WPS-3000TSL autosampler, VF-F11-A-01 Fraction Collector F) (Thermo Fisher Scientific, Waltham, MA, USA) was used. Column: Gemini NX-C18 (5 μm), 250 × 10 mm (Phenomenex, USA).

3.3.3.2 Preparative HPLC separation of compounds from *Linum* species

Mobile phases: 0.1% (v/v) formic acid (A) and ACN (B). Gradient: 0.0 min, 20% B; 50.0 min, 50% B (linear gradient); 55.0 min, 70% B (linear gradient); 90 min, 70% B (isocratic); flow rate: 5.0 mL/min; injected volume: 500 μL. Detection: 280 nm.

3.3.3.3 Preparative HPLC separation of malonyl-dicaffeoylquinic acids from *A. sylvestris*

Mobile phases: 0.1% (v/v) formic acid (A) and ACN (B). Gradient: 0.0 min, 15% B; 4.0 min, 15.0% B (isocratic); 32 min, 25% B (linear gradient); 42.0 min, 90% B (linear gradient); flow rate: 5.0 mL/min; injected volume: 300 μL. Detection: 330 nm.

3.3.3.4 Preparative HPLC separation of lignans from *Anthriscus* species

Mobile phases: 0.1% (v/v) formic acid (A) and 8:2 ACN:0.1% (v/v) formic acid (B). Gradient: 0.0 min, 30% B; 50.0 min, 100% B (linear gradient); 55.0 min, 100% B (linear gradient); flow rate: 5.0 mL/min; injected volume: 500 μL. Detection: 280 nm.

3.4 Compound quantification

3.4.1 *Linum* species

An external standard method was applied using UV (total scan) chromatograms detected in the wavelength range of 230–400 nm. Linear regression analyses of the isolated compounds (linadiacins A, B, diphyllin, and justicidin B) were performed in the range of 0.888–200.0 ng of their injected amounts, resulting in the appropriate r^2 values (higher than 0.9998 for each compound). The amounts of diphyllin glycosides were calculated using the calibration curve of isolated diphyllin.

3.4.2 *Anthriscus* species

An external standard method was employed using UV (total scan) chromatograms detected in the wavelength range of 230–400 nm. Linear regression analyses were performed for the isolated compound, calculating an r^2 value greater than 0.999. (Note: the quantities of compounds **HP-2** and **HP-3** were calculated using the calibration curve of compound **HP-1)**.

3.5 Bioactivity tests (conducted by collaborating partners)

3.5.1 *In vitro* assessment of cytostatic activity of the investigated compounds

The cytotoxic effect of isolated compounds was measured on non-cancerous Vero E6 cells (non-human primate origin; *Cercopithecus aethiops*, kidney, epithelial cells and various human tumor cells using Alamar Blue end-point viability assay.

3.5.2 *In vitro* SARS-CoV-2 inhibitory activity of the investigated compounds

Compounds were evaluated for *in vitro* anti-SARS-CoV-2 activity in non-cancerous Vero E6 cells by measuring viral RNA levels.

3.5.3 Antiadhesive effects in HeLa and preosteoblast cells

The resonant waveguide grating (RWG) technique, employing an evanescent field-based, label-free optical biosensor, was used to investigate the real-time effects of the compounds on cancerous (HeLa) and healthy (preosteoblast) model cells. Cell adhesion kinetics on fibronectin-coated surfaces were analyzed in the presence and absence of the compounds to assess their antiadhesive effects.

3.6 Nuclear magnetic resonance spectroscopy (conducted by a collaborating partner)

NMR spectra were recorded at 25 °C on a Varian DDR spectrometer (599.9 MHz for ^{1}H and 150.9 MHz for ^{13}C) equipped with a dual 5 mm inverse detection gradient (IDPFG) probe-head or at 22 °C on a Bruker Avance III HD 500 (500/150 MHz) spectrometer fitted with a Prodigy cryo-probe head.

4 RESULTS

4.1 Caffeoyl phenylethanoid glycosides from *Forsythia suspensa*

4.1.1 Identification of compounds

The UHPLC-UV-HR-MS separation of the extracts, prepared from the unripe fruit wall of *F. suspensa*, confirmed the presence of three main compounds **S1**–**S3** (**Figure 7**). The HPLC chromatogram shows **S3** to be the most abundant compound in the *Forsythia* extract (**Figure 7**).

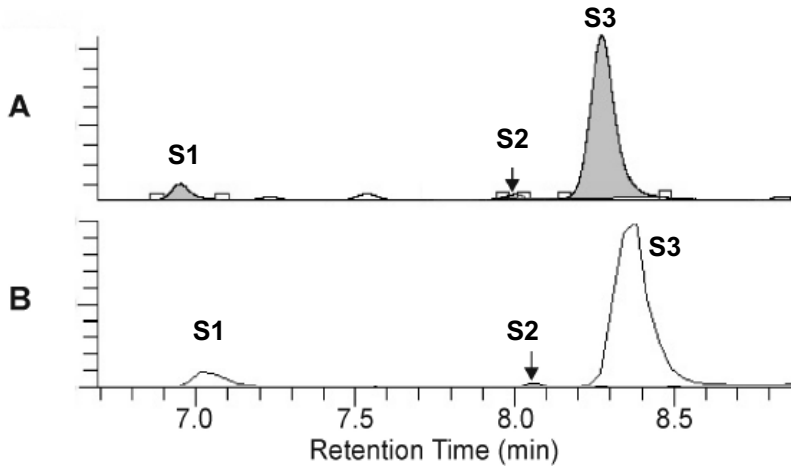

Figure 7. HPLC-UV (λ=330 nm) chromatogram (**A**, retention time window min 6.7–8.8) and extracted ion chromatogram for m/z 623 (**B**) corresponding to the caffeoyl phenylethanoid glycosides forsythoside I (**S1**), forsythoside H (**S2**), forsythoside A (**S3**); adapted from author's own work (110).

Table 2. High-resolution mass-spectral (negative ion mode) data for compounds (**S1**–**S3**) detected in *Forsythia suspensa* fruit wall extracts (author's own table based on own data).

Ret. time[a]	Compounds	Formula	Detected formula	Detected ion	Calculated m/z	Found m/z	diff (ppm)
7.02	S1	$C_{29}H_{36}O_{15}$	$[M-H]^-$	$C_{29}H_{35}O_{15}$	623.19705	623.19733	0.455
8.04	S3	$C_{29}H_{36}O_{15}$	$[M-H]^-$	$C_{29}H_{35}O_{15}$	623.19705	623.19739	0.551
8.38	S4	$C_{29}H_{36}O_{15}$	$[M-H]^-$	$C_{29}H_{35}O_{15}$	623.19705	623.19745	0.647

[a] HPLC-MS retention times (min) of compounds **S1**–**S3**) correspond to those in **Figure 7**.

Comparing molecular formulas, elution properties, and quantitative relationship data with those obtained for already identified compounds of *F. suspensa*, three isomeric CPhEGs, **FI** (**S1**), **FH** (**S2**), and **FA** (**S3**), were previously tentatively identified and now confirmed (**Table 2**).

4.1.2 Mass spectrometry fragmentation study

Fragment ion spectra of **FA**, **FI**, and **FH**, generated from the deprotonated molecular ions of these compounds (i.e., from ion m/z 623) using various collision-induced dissociation (CID) energies (ranging from 20 to 40 eV) were compared: Similar MS/MS fragmentation patterns emerged (**Table 3**, **Figure 8**).

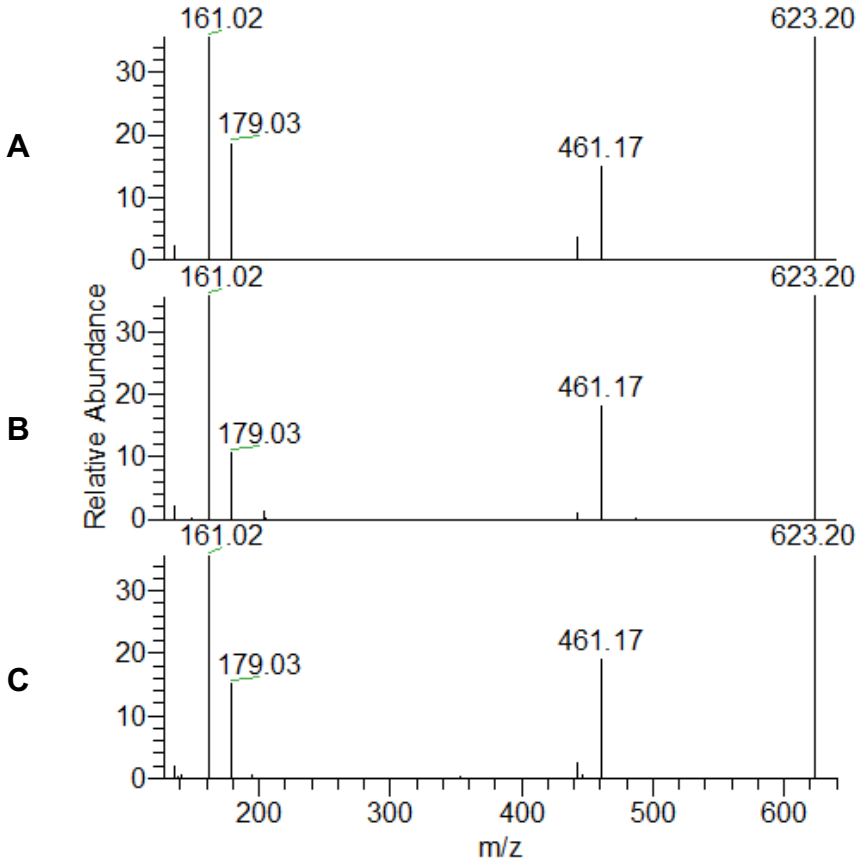

Figure 8. Tandem mass spectra of deprotonated forsythoside A (**A**), forsythoside H (**B**), and forsythoside I (**C**) acquired at a collision-induced dissociation (CID) energy of 30 eV. Ion intensities, expressed as percentages, correspond to values reported in **Table 3**; adapted from authors's own work (110).

Table 3. Relative intensities of characteristic fragment ions generated from deprotonated caffeoyl phenylethanoid glycosides (CPhEGs) forsythoside A (**FA**), forsythoside H (**FH**), and forsythoside I (**FI**), determined by HPLC-HR-MS/MS analysis of an unripe fruit wall extract of *F. suspensa* following collision-induced dissociation (CID) at 20, 31, and 40 eV (author's own table based on own data).

Compound	CID	Intensity[a] of fragment ions, m/z				
		623	461	315	179	161
FA	20 eV	100.0	0.80	-	0.50	3.1
	30 eV	100.0	15.0	-	18.1	63.0
	40 eV	8.1	10.0	0.30	24.0	100.0
FH	20 eV	100.0	1.3	-	-	3.0
	30 eV	100.0	20.0	-	12.0	72.5
	40 eV	6.0	10.0	0.70	16.2	100.0
FI	20 eV	100.0	0.91	-	0.44	3.3
	30 eV	100.0	19.0	-	16.0	80.0
	40 eV	5.5	8.2	0.48	17.0	100.0

[a] Intensities are expressed as percentages relative to the most intense ion in the MS/MS spectrum within the m/z range of 130–650.

4.2 Arylnaphthalene lignans from *Linum austriacum* and *L. perenne*

4.2.1 Identification of compounds and conversion study

Pulverized rhizome and root tissues of *L. austriacum* were first subjected to different treatments, including acidic (2 M TFA, 100 °C for 3 and 30 min) and endogenous enzymatic (incubation in water for 30 min at room temperature) procedures, followed by extraction. The resulting extracts, together with untreated samples, were analyzed by HPLC-UV-HR-MS/MS. Intact tissue extracts were also prepared using hot methanol.

The HPLC-UV-HR-MS/MS analysis revealed eight major compounds (**1**–**8**) in extracts of *L. austriacum* roots and rhizomes obtained under the distinct treatment conditions (**Figure 9**). Compounds exhibiting comparable retention times across

chromatograms **A**–**F** showed consistant molecular formulas and tandem mass spectra, confirming their identical chemical structures (**Table 4**, **Figure 9**).

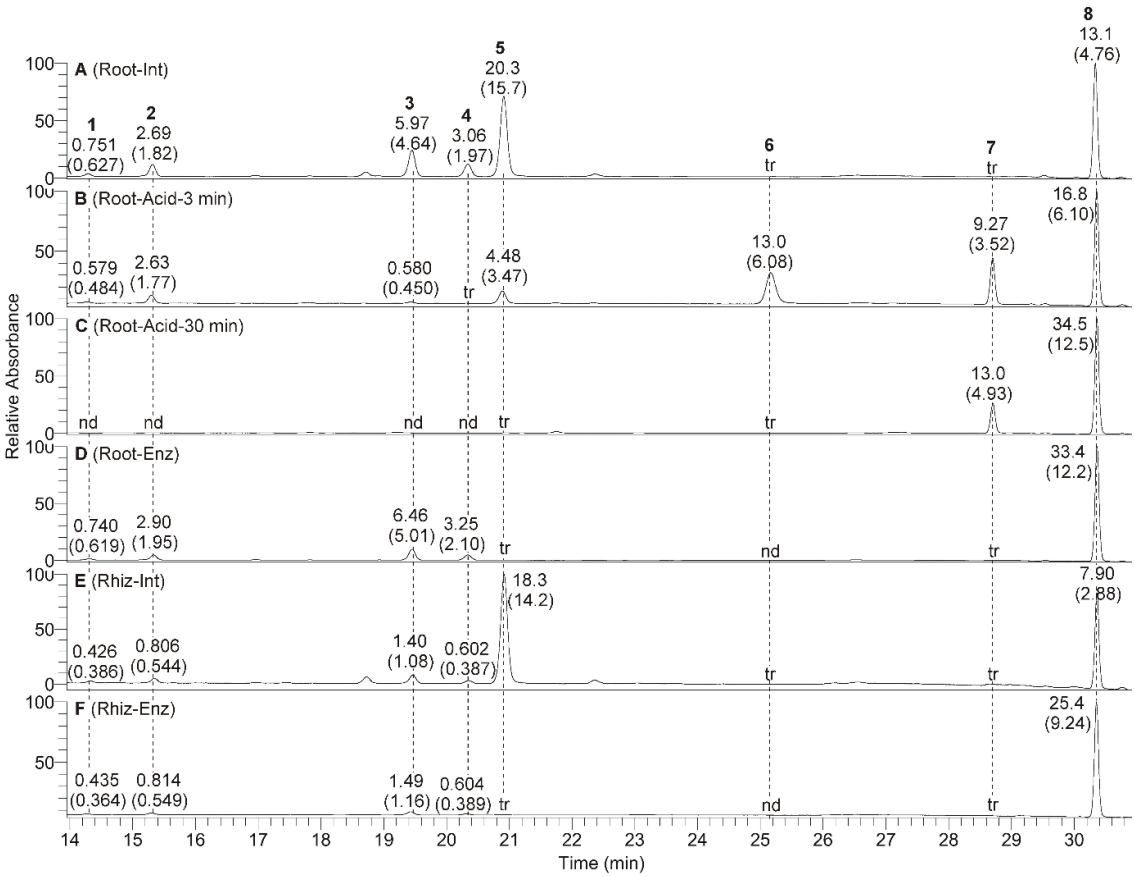

Figure 9. HPLC-UV (λ=230–400 nm, total scan) chromatograms (retention time window min 14.0–31.0) of the *Linum austriacum* root (**A**–**E**) and rhizome (**E**, **F**) extracts. Intact root (**A**, **Root-Int**) and rhizome (**E**, **Rhiz-Int**) samples, their enzyme-treated counterparts (**D**, **Root-Enz** and **F**, **Rhiz-Enz**, respectively) and root extracts after 3 min (**B**, **Root-Acid-3 min**), and 30 min (C, **Root-Acid-30 min**) of acid treatments (in 2 M trifluoroacetic acid at 100 °C) were analyzed. Amounts of compounds in the dried samples, expressed in μmol/g (printed in normal) and mg/g (printed in parentheses) values, are also indicated (**tr**, trace amounts are below calibration range; **nd**, not detected). Intact root and rhizome samples correspond to those collected in September that are marked with **A1** in **Table 5**. The amounts of compounds in the intact and enzyme-treated root and rhizome samples are the averages of three separate experiments, and the differences, characterized by the relative standard deviation (RSD) values, were less than 4.9%; adapted from author's own work (111).

Table 4. Relative intensities of characteristic ions in the full mass spectra (MS1) and in the tandem mass spectra (MS2) of linadiacins A and B (compounds **5** and **6**), determined by HPLC high-resolution Orbitrap-MS and MS/MS using negative and positive ionization modes; adapted from author's own work (111).

Mode[a]	No, Name	Analysis	CID[b] (eV)	Relative intensities (%)[c] of characteristic ions (CIs)[d] indicated by mass-to-charge ratios (*m/z*)[e]								
negative	**5**, linadiacin A			CI→	[c-H]$^-$	[linadiacin B-H-CO_2]$^-$	[b-H-CO_2]$^-$	[M-H-CO_2]$^-$			[M-H]$^-$	
				m/z→	381.0969	423.1074	585.1603	729.2025			773.1924	
		MS1			-	-	-	2.61			93.5	
			10		-	4.8	0.51	44.4			16.9	
		MS2	20		0.18	7.1	0.12	5.7			-	
			30		0.30	0.68	-	-			-	
	6, linadiacin B			CI→		[c-H]$^-$		[M-H-CO_2]$^-$			[M-H]$^-$	
				m/z→		381.0969		423.1074			467.0973	
		MS1				57.8		6.7			10.4	
			10			58.3		-			-	
		MS2	20			24.2		-			-	
			30			-		-			-	
positive	**5**, linadiacin A			CI→	[justicidin B+H]$^+$	[a-4×H_2O]$^+$	[a-3×H_2O]$^+$	[a-2×H_2O]$^+$	[a-H_2O]$^+$	[a]$^+$	[M+NH_4]$^+$	[M+Na]$^+$
				m/z→	365.1020	599.1548	617.1654	635.1759	653.1865	671.1970	792.2346	797.1899
		MS1			14.4	-	0.020	0.24	0.90	1.92	38.9	9.11
			10		47.6	0.033	0.84	2.2	5.9	10.7	17.6	
		MS2	20		78.6	0.22	0.95	0.64	0.83	0.36	0.080	
			30		93.5	0.31	0.37	-	-	-	-	
	6, linadiacin B			CI→	[justicidin B+H]$^+$			[M+NH_4]$^+$			[M+Na]$^+$	
				m/z→	365.1020			486.1395			491.0949	
		MS1			42.7			32.7			4.8	
			10		97.1			-				
		MS2	20		95.7			-				
			30		61.7			-				

[a] Negative and positive ionization modes were used (polarity switching mode). [b] Fragmentations of deprotonated ions and ammonium adducts of both compounds were analyzed by parallel reaction monitoring (PRM) method using collision-induced dissociation (**CID**) energies of **10 eV**, **20 eV**, and **30 eV**. [c] Expressed as percentages of the total fragment ion intensity. [d] Structures of fragment ions indicated by symbols **a**, **b**, and **c**, are shown in **Figure 18**. [e] Calculated masses; the differences between the calculated masses of the characteristic ions (**CIs**) and the measured masses of the corresponding ions were less than 5.0 ppm.

Comparison with previously reported data for *L. austriacum* and *L. perenne* confirmed the presence of diphyllin (**7**), justicidin B (**8**), and four glycosides, i.e., a pentosyl-dihexoside (**1**), a pentosyl-monohexoside (**2**), a tripentoside (**3**), and a dipentoside (**4**) of diphyllin in the root tissues of *L. austriacum* (**Figure 10**) (19,95). In contrast, no previously reported metabolites from *Linum* species could be assigned to molecular formulas of compounds **5** ($C_{36}H_{38}O_{19}$) and **6** ($C_{24}H_{20}O_{10}$) (**Table 4**).

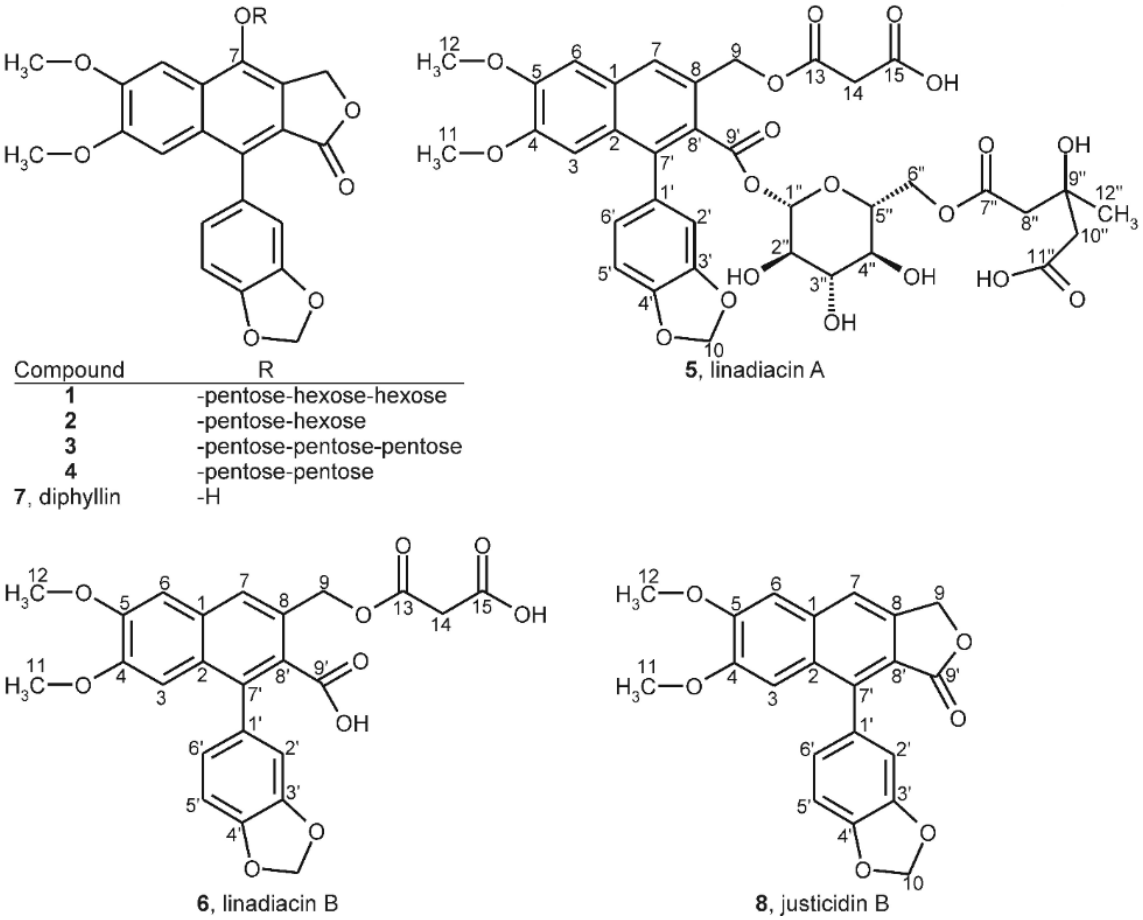

Figure 10. Chemical structures of compounds **1**–**8** identified in *Linum austriacum* and *L. perenne* extracts; adapted from author's own work (111).

Structure-specific data for the identification of compounds **5** and **6** were obtained through a conversion study and results were quantitatively evaluated. For these purposes, calibrations were performed using pure compounds isolated from their optimum raw materials (Section **4.2.2**). Comparing the chromatograms of the untreated, intact root sample (**Root-Int**) with its acid- (for 30 min) and enzyme-treated counterparts (**Root-Acid-30 min** and **Root-Enz**), it can be stated that compound **5** is unstable, as its complete decomposition is observed, which was followed by an increasing in the amount of justicidin B (peak **8**) during both treatments (**Figure 9**). The increases in justicidin B observed after acidic (21.4 µmol/g) and enzymatic (20.3 µmol/g) treatments, corresponding to the differences between the **Root-Acid-30 min** and **Root-Int** samples and between the **Root-Enz** and **Root-Int** samples, matched the initial amount of compound **5** in the intact extract (20.3 µmol/g), confirming its quantitative conversion

into justicidin B under these conditions (**Figure 9**). A quantitative enzymatic conversion of compound **5** into justicidin B was also detected in the rhizome samples (**Figure 9**, **Rhiz-Int** versus **Rhiz-Enz**). Justicidin B lacks free hydroxyl groups; therefore, its formation cannot be rationalized by common lignan conversion pathways such as acidic or enzymatic hydrolysis of glycosidic bonds. Moreover, short-term heating (3 min) in an acidic medium resulted in the formation of one additional compound (**6** in sample **Root-Acid-3 min**, **Figure 9**), demonstrating a two-step formation of justicidin B via intermediate product **6**. Compound **6** was also found present in the intact tissues but only in trace amounts. The glycosides of diphyllin (compounds **1**, **2**, **3**, and **4**) were hydrolyzed by acid treatment (in 2 M TFA at 100 °C), forming their aglycone diphyllin. This conversion was quantitative, as the yield of diphyllin in the sample heated in an acidic medium for 30 min (**Root-Acid-30 min**, 13.0 µmol/g) correlated with the total amount of diphyllin glycosides (∑ 12.5 µmol/g) in the intact extract (**Root-Int**, **1**, **Figure 9**).

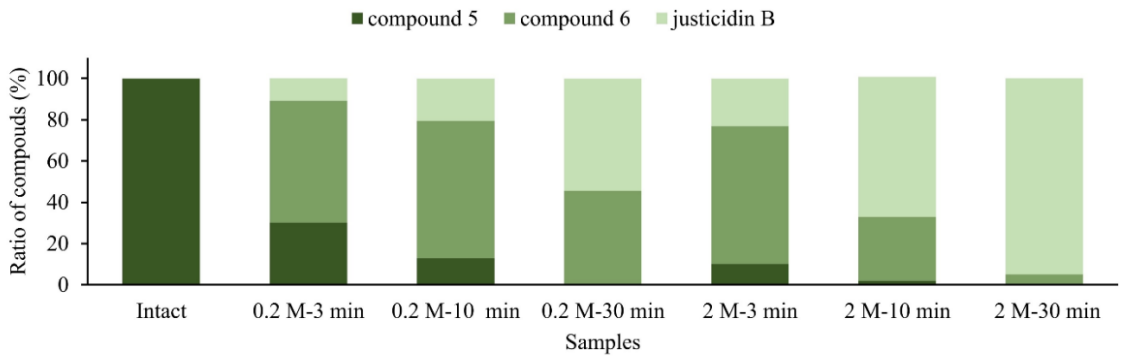

Figure 11. Effect of acid treatment on the aliquots of isolated compound **5** (**Intact**) that were heated at 100 °C for 3 min, 10 min, and 30 min with 0.2 M (**0.2 M-3 min**, **0.2 M-10 min, 0.2 M-30 min**) and 2 M trifluoroacetic acid (**2 M-3 min**, **2 M-10 min**, **2 M-30 min**). Amounts of compounds are expressed in percentages (%), calculated from the µmol values of compounds in the samples as follows: the amount of a compound in the sample (µmol) was divided by the total amount of compounds (µmol) in the same sample × 100; adapted from author's own work (111).

The effects of the acid treatments on pure compound **5** isolated from its optimum raw material were more extensively studied, aiming to confirm this two-step conversion and to prepare compound **6** at the highest yield possible, allowing its isolation. Aliquots of compound **5** (1.00 µmol) were heated at 100 °C in 0.2 M and 2 M TFA for various periods (3 min, 10 min, and 30 min) (**Figure 11**). The results showed a relatively fast

conversion of compound **5** into compound **6** that was followed by a slower decomposition of compound **6**, forming justicidin B as the final product of this two-step reaction (**Figure 11**). The total amounts of the conversion products (compound **6** and justicidin B) together with the remaining compound **5** in samples heated in 0.2 M and 2 M TFA for different time periods ranged from 0.950 to 1.06 µmol. These values were comparable to the starting amount of compound **5** (1.00 µmol) and within the experimental error of HPLC-UV quantitation (**Figure 9**), indicating that the quantitative two-step conversion to compound **6** and justicidin B proceeded without detectable degradation.

4.2.2 Selection of optimal tissues for isolation of compounds

To identify the optimal tissues for described methods and particularly isolation, the metabolite composition in the underground organs (i.e., in roots and rhizomes) of wild-grown *L. austriacum* and of *L. perenne* was also analyzed during a full vegetation cycle of one year by HPLC-UV-HR-MS. All extracts exhibited a uniform metabolite profile comprising diphyllin glycosides (**1**–**4**), free diphyllin (**7**), and justicidin B (**8**) as well as the identiefied compounds **5** and **6** (**Table 5**).

Compound **5** was observed as the predominant compound in all samples, whereas compound **6** and diphyllin were present only in trace amounts. HPLC-UV-MS analysis of isolated compound 5 indicated a purity of 81.0%, with **4** (19.0% w/w) present as a co-eluting compound. Despite method optimization to achieve baseline separation, compounds **5** and **4** could not be efficiently resolved by preparative HPLC. Comparison of compounds **5** and **4** in root and rhizome samples showed higher **5/4** ratios in rhizomes (average 32.5) than in roots (average 8.4), indicating a lower relative abundance of compound **4** (co-eluting compound) at higher ratio values (**Table 5**). Thus, compound **5** was isolated from the rhizome sample (***L. au.***, sample **A1**, **September**) by preparative HPLC with a purity of 96.9% (**Table 5**). It was subsequently used for structural elucidation and bioactivity evaluation.

According to the conversion behavior of diphyllin glycosides and compound **5** in acidic media, a root sample with high levels of these compounds (***L. au.***, sample **A1**, **September**) was selected for acid treatment and isolation (**Table 5**).

Table 5. Composition of the dried underground organ samples of *L. austriacum* (***L. au.***) and *L. perenne* **(*L. pe.*)**, determined during a full vegetation cycle of one year by HPLC-UV-MS; adapted from author's own work (111).

Coll. time[a]	Species	Tissue	Coll. locat[b]	Amounts of compounds (**1**–**8**) in the dried tissues (mg/g)						Ratio, **5**/**4**[d]
				Sum of diphyllin glycosides **1**–**4**[c]	**4**	**5**	**6**	**7**	**8**	
April	*L. au.*	root	A1	11.1	3.14	25.6	tr	tr	4.14	8.2
		rhizome		1.73	0.319	9.96	tr	tr	1.22	31.2
	L. pe.	root	P1	8.00	3.11	23.8	0.390	tr	4.85	7.7
		rhizome		1.99	0.790	15.4	0.264	tr	2.19	19.5
June	*L. au.*	root	A1	9.91	2.10	20.0	tr	tr	5.43	9.5
		rhizome		0.743	0.159	7.58	tr	tr	1.17	47.7
		root	A2	10.5	2.04	23.1	tr	tr	5.46	11.3
		rhizome		1.89	0.390	16.3	tr	tr	2.43	41.8
	L. pe.	root	P1	15.4	3.02	23.0	tr	tr	9.71	7.6
		rhizome		3.28	0.568	16.1	tr	tr	3.97	28.3
September	*L. au.*	root	A1	9.59	2.14	15.8	tr	tr	4.99	7.4
		rhizome		2.44	0.408	14.1	tr	tr	3.04	34.6
		root	A3	9.05	2.40	13.9	tr	tr	7.38	5.8
		rhizome		1.86	0.39	9.91	tr	tr	2.80	25.4
	L. pe.	root	P2	11.1	2.61	16.2	tr	tr	4.05	6.2
		rhizome		2.68	0.569	11.9	tr	tr	1.79	20.9
December	*L. au.*	root	A1	7.31	1.49	10.7	tr	tr	2.39	7.2
		rhizome		1.97	0.337	7.29	tr	tr	1.22	21.6
	L. pe.	root	P1	7.43	1.33	17.2	tr	tr	2.79	12.9
		rhizome		1.91	0.213	11.5	tr	tr	1.32	54.0

[a] Collection time; plant samples were collected four times (in **April**, **June**, **September**, and **December**), during a full vegetation cycle of one year. [b] Sample collection location; samples marked with **A1**–**A3** and **P1**, **P2** were collected from different Hungarian locations of *L. austriacum* and *L. perenne*, respectively. [c] Total amounts of diphyllin glycosides were calculated by adding the amounts of compounds **1**, **2**, **3**, and **4**. [d] Quantitative ratios between compounds **5** and **4**, calculated by dividing amounts of **5** by amounts of **4**; **tr**, trace amounts are below calibration range.

Extracts were treated with 2 M TFA for 3 min to enrich compound **6** and for 30 min to achieve complete hydrolysis of glycosides to diphyllin, followed by preparative HPLC isolation and subsequent structural confirmation and bioactivity studies.

Based on NMR results from a collaborating research group, compounds **5** and **6** were identified as new natural AN lignan derivatives, designated linadiacin A and linadiacin B, respectively (**Table 4**, **Figure 10**).

4.2.3 *In vitro* SARS-CoV-2 inhibitory activity of arylnaphthalene lignans isolated from *Linum* spp.

The AN lignans designated linadiacin A and linadiacin B as well as known diphyllin and justicidin B, all isolated from selected tissues after the optimized acidic treatments, were evaluated for their *in vitro* anti-SARS-CoV-2 potential by a collaborating research group using the non-cancerous Vero E6 cells as hosts.

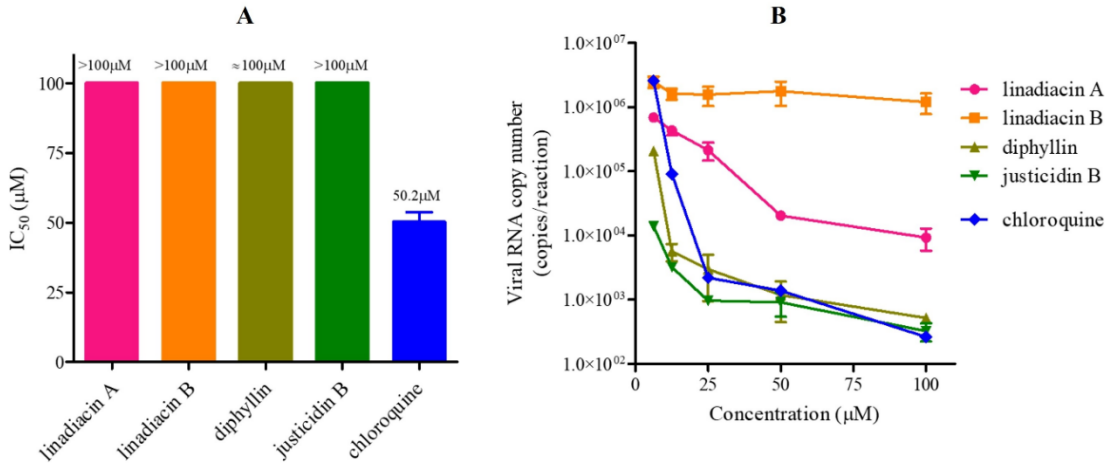

Figure 12. Cytotoxic (panel **A**) and antiviral (panel **B**) activity of the isolated compounds against the non-cancer host cells Vero E6 and Severe Acute Respiratory Syndrome Coronavirus 2 (SARS-CoV-2), respectively (IC_{50} values are compound concentrations required for 50% inhibition of the cell viability); adapted from author's own work (111).

Linadiacins A and B showed no cytotoxicity on Vero E6 cells for up to 100 μM concentration. Diphyllin and justicidin B reduced Vero E6 cell viability by 48% and 25%, respectively, even at the highest concentration tested (100 μM). The dose-dependent activity of linadiacin A, diphyllin, and justicidin B and the inactivity of linadiacin B against the SARS-CoV-2 virus were confirmed in the concentration range from 6.25 μM to 100 μM by quantifying the viral RNA copy number (**Figure 12**).

4.2.4 Antiproliferative activity of arylnaphthalene lignans isolated from *Linum* spp.

The antiproliferative activity of isolated compounds was confirmed against six various human cancer cell cultures, i.e., four lung cancer cell lines (A549, Calu-1, Ebc-1, H838), one melanoma cell line (A2058), and one prostate cancer cell line (PC-3) by a collaborating research group. Both compounds **5** and **6** exhibited antiproliferative activity, particularly in EBC-1, A2058, and PC-3 cells (**Figure 13**).

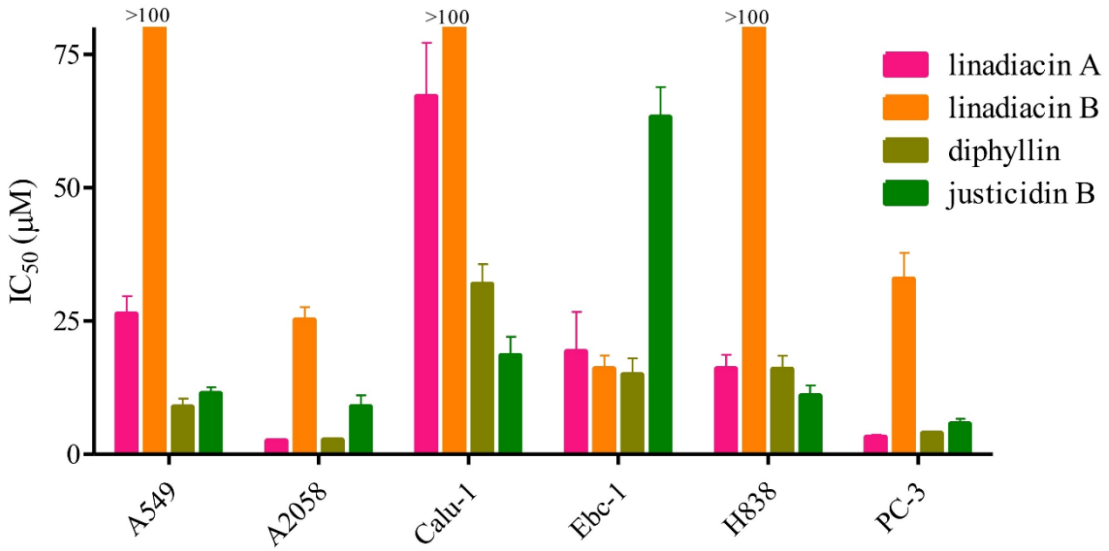

Figure 13. Antiproliferative effect of the isolated compounds against human lung cancer cell lines (A549, Calu-1, Ebc-1, H838), as well as human melanoma (A2058) and prostate cancer (PC-3) cells; adapted from author's own work (111).

4.3 Lignans and malonyl-dicaffeoylquinic acids from *Anthriscus* spp.

4.3.1 Identification of aryltetralin and dibenzylbutyrolactone lignans

Various organs (roots, leaves, and inflorescences) of *A. caucalis*, *A. nitida*, and *A. sylvestris* were analyzed using HPLC-UV-HR-MS/MS. Compounds detected within the retention time window of 12.5–17.0 min exhibited UV and HR-MS spectral characteristics comparable to those of the lignans desmethylyatein (**DeMeYA**), dimethylmatairesinol (**DiMeMAT**), deoxypodophyllotoxin (**DPT**), yatein (**YA**), kaerophyllin (**KAP**), anhydropodorhizol (**AHP**), and angeloyl podophyllotoxin (**APT**), listed in order of increasing retention time (**Figures 14** and **15**) (11, 22-24).

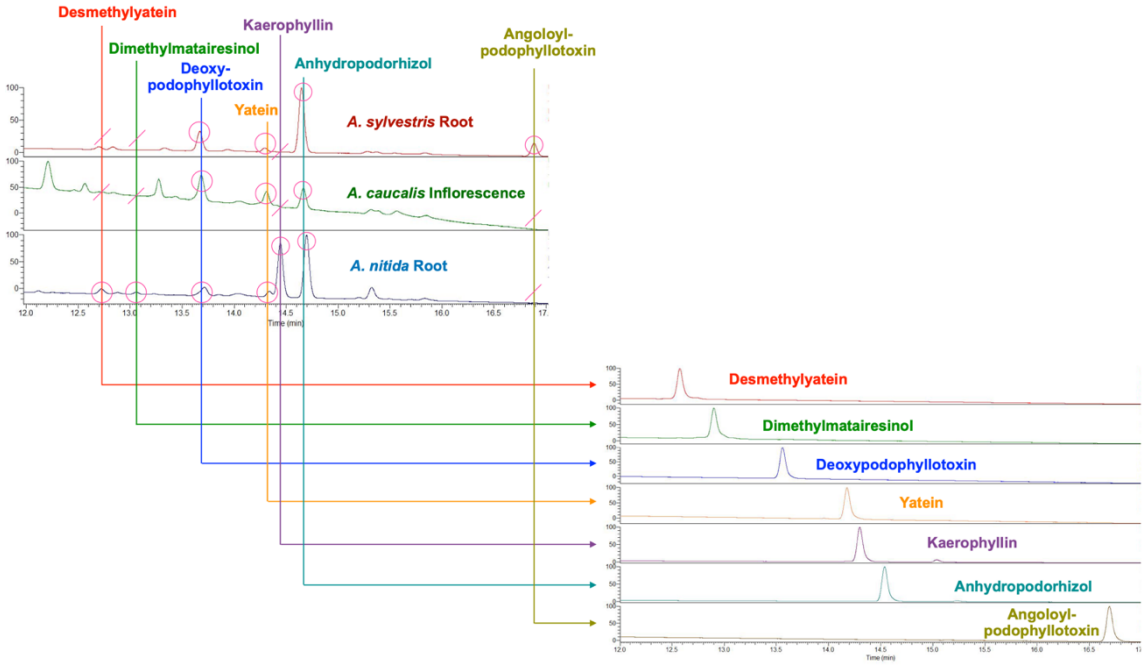

Figure 14. HPLC-UV chromatograms (retention time window min 12.0–17.0) of extracts prepared from the roots of *A. sylvestris* and *A. nitida* and from the inflorescence of *A. caucalis*, together with the HPLC-UV chromatograms (retention time window min 12.0–17.0) of the isolated lignans (author's own graph based on own data).

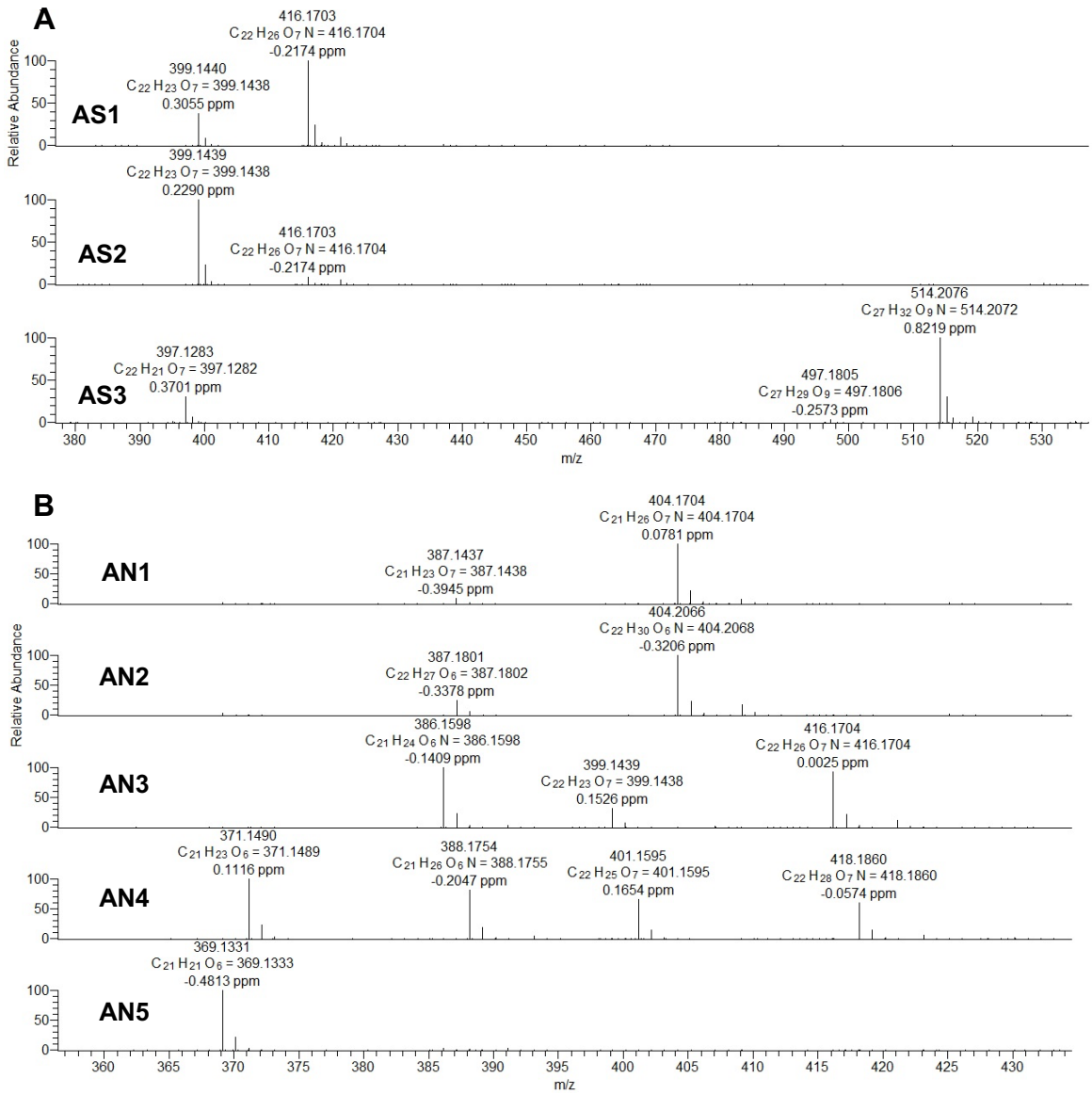

Figure 15. Mass spectra of lignans identified in *A. sylvestris* (panel **A**) and *A. nitida* (panel **B**), along with the calculated molecular formulas and difference values between calculated and measured masses (expressed in ppm values). Compounds **AS1**–**AS3** correspond to deoxypodophyllotoxin (**AS1**), anhydropodorhizol (**AS2**), angeloyl podophyllotoxin (**AS3**), Compounds **AN1**–**AN5** correspond to desmethylyatein (**AN1**), dimethylmatairesinol (**AN2**), deoxypodophyllotoxin and an impurity (**AN3**), yatein and an impurity (**AN4**), kaerophyllin (**AN5**). Note: **AN3** and **AN4** are mixtures of compounds that could not be separated. The spectra were acquired using electrospray ionization (ESI) in positive ionization mode; adapted from author's own work.

4.3.2 Malonyl-dicaffeoylquinic acids from *A. sylvestris*

In the HPLC–UV chromatogram of the *A. sylvestris* leaf extract collected at the beginning of the vegetation cycle (**Figure 16**), two peaks were observed at retention times of 7.3 and 7.6 min. These retention times are substantially shorter than those of the lignans, which are relatively apolar and elute between 12.5 and 17.0 min (**Figure 14**), indicating that the compounds eluting at 7.3 and 7.6 min are highly polar (**HP**). Tandem mass spectra of the later-eluting polar peak (7.6 min) revealed the presence of co-eluting compounds. After application of a modified gradient program, this region was resolved into two distinct peaks, designated **HP-2** and **HP-3**, while the earlier-eluting compound remained a single, well-defined peak under both gradient conditions and was designated **HP-1**.

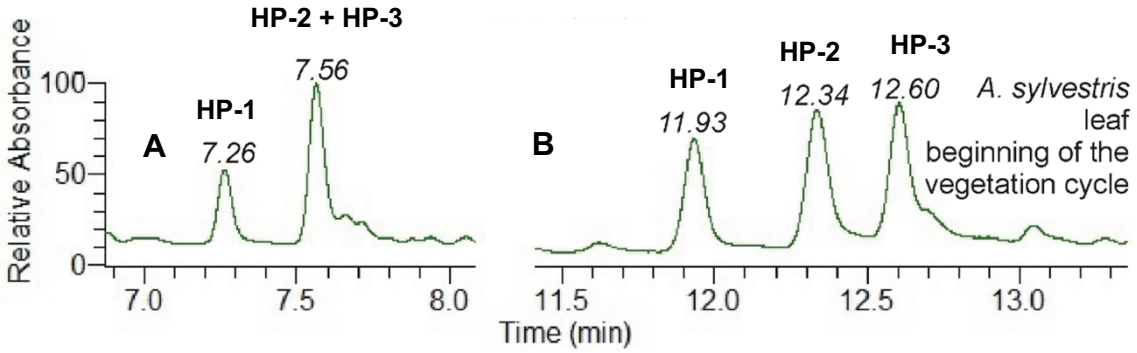

Figure 16. HPLC-UV (λ = 230–600 nm, total scan) chromatogram (retention time window min 6.9–8.1 **A**; min 11.4–13.3 **B**) *A. sylvestris* (**A**, **B**) extract using both gradient program 1 (**A**) and gradient program 2 (**B**). The extract was prepared from the leaves collected at the beginning of the vegetation cycle. Peak numbers (bold) correspond to the numbering of the identified compounds, with retention times (min) indicated in italics; adapted from author's own work (113).

High-resolution MS spectra of **HP-1**, **HP-2**, and **HP-3** were comparable (**Table 6**) and allowed assignment of the same molecular formula, $C_{28}H_{25}O_{15}$. This formula is consistent with malonyl-dicaffeoylquinic acids, which were previously tentatively identified in *A. cerefolium* without definitive structural confirmation (**Figure 5**).

Table 6. Mass spectrometry (MS) data of malonyl-dicaffeoylquinic acids (MDiCQAs), obtained from the mass spectra of these compounds, determined by HPLC-HR-MS using negative and positive electrospray ionization (ESI) modes; adapted from author's own work (113).

compound[a]	formula	measured and calculated masses (*m/z*) of ions and the difference (ppm)[b] between them		
		ionization mode: positive		
		detected ions[c]	$[M+H]^+$	$[M+NH_4]^+$
	$C_{28}H_{26}O_{15}$	calculated mass	603.1344	620.1610
HP-1		measured mas	603.1338	620.1603
		mass error	-1.088	-1.057
HP-2		measured mass	603.1342	620.1612
		mass error	-0.475	0.314
HP-3		measured mass	603.1335	620.1601
		mass error	-1.602	-1.444
		ionization mode: negative		
		detected ions[c]	$[M-H]^-$	
	$C_{28}H_{26}O_{15}$	calculated mass	601.1199	
HP-1		measured mass	601.1198	
		mass error	-0.138	
HP-2		measured mass	601.1205	
		mass error	1.076	
HP-3		measured mass	601.1207	
		mass error	1.292	

[a] Highly polar malonyl-dicaffeoylquinic acids are marked by **HP-1**, **HP-2**, and **HP-3**.

4.3.2.1 Malonyl-dicaffeoylquinic acid composition in different tissues of *A. sylvestris*

The composition of MDiCQAs was analyzed in inflorescence, leaf, and root tissues of *A. sylvestris* during the flowering stage. In addition, leaf and root tissues were examined at the beginning of the vegetation cycle (**BVC**) in early spring (**Table 7**). The results revealed pronounced tissue-dependent differences in MDiCQA accumulation. Compounds **HP-2** and **HP-3** accumulated predominantly in leaves at the **BVC**, where they reached their highest concentrations (2.08 mg/g for **HP-2** and 1.91 mg/g for **HP-3**, both in **AS-L-BVC-1**), and were present only at low levels in inflorescences and roots. In contrast, compound **HP-1** was also detected at high concentrations in inflorescence samples (**Table 7**).

Table 7. Composition of dried leaf, inflorescence, and root samples of *Anthriscus sylvestris* collected at the beginning of the vegetation cycle and in the flowering stage, determined by HPLC-UV; adapted from author's own work (113).

Tissue	Coll. time[a]	Coll. locat.[b]	Sample name[c]	Amounts of compounds in the dried tissues (mg/g)		
				HP-1	**HP-2**	**HP-3**
Leaf	BVC	1	AS-L-BVC-1	1.79	2.08	1.91
		2	AS-L-BVC-2	3.29	1.20	0.78
		5	AS-L-BVC-5*A*	1.98	1.25	0.79
		5	AS-L-BVC-5*B*	1.93	1.20	0.81
	FS	1	AS-L-FS-1	2.47	-	-
		2	AS-L-FS-2	1.45	0.12	0.23
		4	AS-L-FS-4	2.64	-	-
Inflores-cence	FS	1	AS-I-FS-1	6.70	-	-
		2	AS-I-FS-2	2.85	0.36	0.28
		3	AS-I-FS-3	2.93	0.62	0.57
		4	AS-I-FS-4	2.46	0.18	0.17
Root	BVC	1	AS-R-BVC-1	1.80	0.59	0.10
		5	AS-R-BVC-5	1.32	0.28	0.15
	FS	1	AS-R-FS-1	2.71	0.22	0.11
		3	AS-R-FS-3	3.52	0.22	0.10

[a] Collection time: Samples were collected at the beginning of the vegetation cycle (from January to March) (**BVC** samples) and in the flowering stage (May) (**FS** samples) of *Anthriscus sylvestris*. [b] Sample collection location: plant samples were collected from different Hungarian locations marked with numbers **1**–**5**. [c] Sample name abbreviations refer to the plant species (**AS**–*Anthriscus sylvestris*), analyzed tissue (**L**–leaf, **I**–Inflorescence, or **R**–root), collection time (**BVC**–beginning of the vegetation cycle, or **FS**–flowering stage), and independent extraction parallel (**A** and **B** printed in italic).

4.3.2.2 Antiproliferative activity of malonyl-dicaffeoylquinic acids isolated from *A. sylvestris*

The antiproliferative activity of the isolated MDiCQAs **HP-1**, **HP-2**, and **HP-3** was evaluated against healthy Vero E6 cells and a panel of human cancer cell lines. The IC_{50} values of compounds **HP-2** and **HP-3** exceeded 100 μM for all tested cell lines; therefore, these compounds are not included in **Table 8**.

Table 8. Cytostatic compound **HP-1** on **Vero E6** cells and human colorectal carcinoma (**HT-29**), glioma (**U87**), hepatoblastoma (**HepG2**), leukemia (**HL-60**), and melanoma (**A2058**). Results are presented as means ± SD, calculated from four parallel tests performed two times independently. Reproduced with permission from Nazli A (108).

cell line	IC_{50} (μM)[a]	
	HP-1	Daunomycin
Vero E6	9.9 ± 1.4	1.7 ± 0.5
A2058	13.5 ± 1.5	0.2 ± 0.01
U87	>100	0.6 ± 0.05
HL-60	29.7 ± 4.6	0.16 ± 0.03
HepG2	25.6 ± 2.3	0.54 ± 0.15
HT-29	>100	0.9 ± 0.1

5 DISCUSSION

5.1 Caffeoylphenylethanoid glycosides from *Forsythia suspensa*

Fragment ion spectra of **FA**, **FI**, and **FH**, generated from the deprotonated molecular ions of these compounds (m/z 623) using collision-induced dissociation (CID, 35 eV), exhibited identical fragment ions for these isomeric CPhEGs, confirming their structures but not allowing discrimination between them (**Table 3**, **Figure 17**).

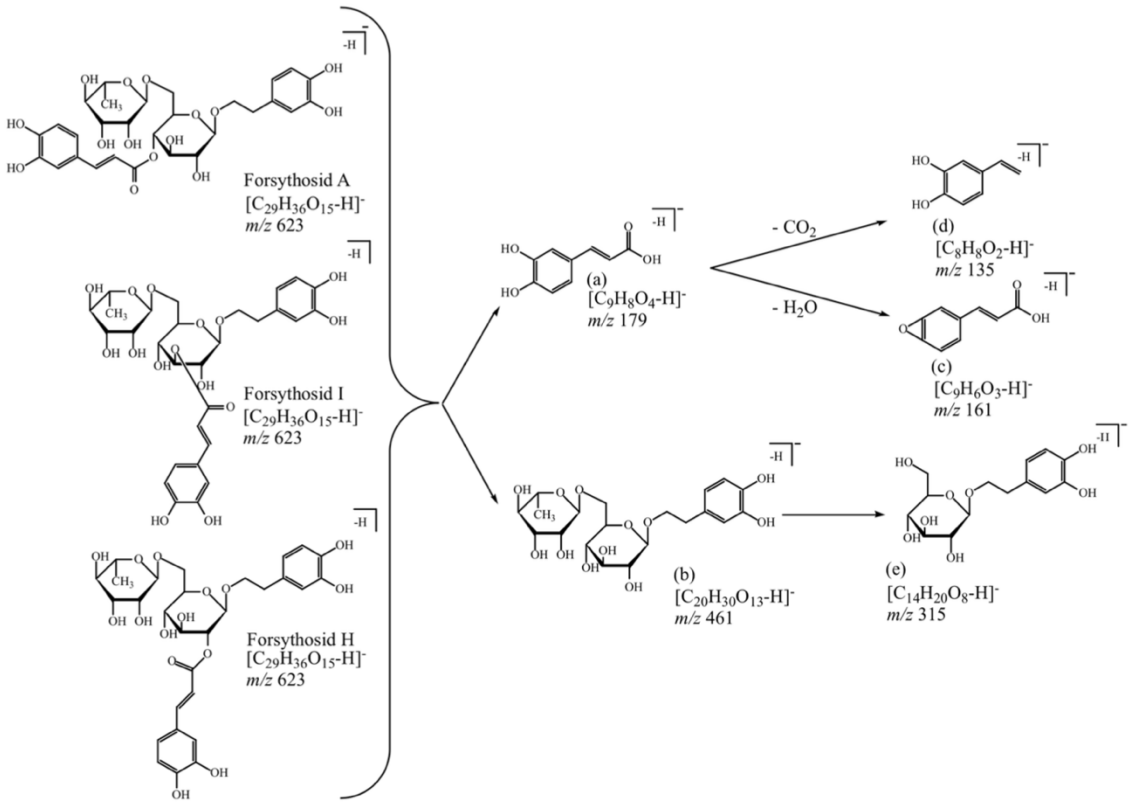

Figure 17. Proposed fragmentation pathways of forsythoside isomers. Reproduced with permission from Zürn M (109).

5.2 Arylnaphthalene lignans from *Linum austriacum* and *L. perenne*

5.2.1 Identification, conversion and isolation of compounds

The identification of identical compounds **1**–**8** in different concentrations after various treatments suggests that these compounds undergo treatment-dependent conversion processes (**Figure 9**). Disruption of tissue compartmentalization by pulverization enables effective interaction between endogenous enzymes (e.g.,

glycosidases) and their substrates, thereby facilitating enzymatic transformations in aqueous media. The observed quantitative hydrolysis of lignan glycosides within 30 min is consistent with previous reports and confirms the efficiency of this approach for inducing endogenous conversions (29,94). The detection of diphyllin, justicidin B, and their glycosides is in agreement with earlier studies on *Linum* species, supporting the reliability of the analytical approach (19,95). In contrast, the occurrence of compounds **5** and **6**, which could not be assigned to previously reported metabolites, suggests the presence of novel AN lignan derivatives and highlights the potential of these tissues as a source of previously uncharacterized bioactive compounds. Because relatively high amounts of before not assignable compound **6** were detected in the sample heated with 2 M TFA for 3 min, 0.2 M TFA for 3 min and 10 min, these treatment conditions can be used to prepare this compound before its preparative HPLC isolation (**Figure 11**). The conversion of new compound **5** into justicidin B (**8**) via intermediate **6** and the tandem MS detection of similar characteristic ions suggests they have closely related structures containing the same basic skeleton (**Table 4**, **Figure 9**). However, as detailed above, a quantitative enzymatic conversion of compound **5** into compound **8** could be confirmed in the root and rhizome samples. Comparing the impact of the enzymatic and acidic treatment conditions on the formation of compound **8** from compound **5**, we can state that compound **6**, which was generated as an intermediate product during the acid treatment, was not formed by the enzymatic processes even when using shorter treatment times. Thus, optimized acid treatment procedures enable the enrichment of the novel compound **6** from tissues of *L. austriacum* and *L. perenne*, highlighting their suitability as source materials (**Figure 11**). Based on the observed conversion behavior of diphyllin glycosides **1**–**4** and compound **5** under acidic conditions, a root sample (***L. au***., **A1**, **September**) containing high levels of these compounds was selected for subsequent acid treatment and isolation (**Table 5**). Compound **5** was identified as the major constituent in all samples in **Table 5**, although minor amounts of the diphyllin glycoside **4** were present as a co-occurring impurity in intact extracts. Its isolation at high purity (96.9%) was achieved by selecting tissues with elevated 5/4 ratios, an approach enabled by the investigation of AN lignan composition over the course of a full vegetation cycle (**Table 5**). Justicidin B can be isolated from both intact and treated extracts, with substantially

higher yields following enzymatic and acidic treatments, consistent with its role as the final conversion product of compounds **5** and **6**.

The amount of diphyllin in the intact sample was negligible, and its isolation was therefore only feasible following quantitative acid hydrolysis of samples containing high levels of diphyllin glycosides (**Table 5**). Notably, although many lignan glycosides can be hydrolyzed by endogenous glycosidases, diphyllin glycosides remained stable under the applied enzymatic treatment conditions.

5.2.2 Mass fragmentation study of linadiacin A and linadiacin B

Mass fragmentations of linadiacins A and B were performed by HPLC-HR-MS/MS using negative and positive ionization modes and various collision induced dissociation (CID) energies (10 eV, 20 eV, and 30 eV). The mass fragment spectra of the deprotonated ion m/z 773 of linadiacin A (**Table 4**) showed characteristic fragment ions with m/z 585 and m/z 423, which confirm the consecutive elimination of hydroxy-methylglutaryl (**x_1**, **Figure 18**) and glucosyl (**x_2**, **Figure 18**) moieties accompanied by the decarboxylation of the malonyl group. After these fragmentation steps, the decarboxylated malonyl unit was also eliminated (**x_3**, **Figure 18**), as evidenced by the formation of the m/z 381 ion (**Table 4**). The ion m/z 423, appearing as an intermediate in the fragmentation pathway of linadiacin A, is identical to the decarboxylated linadiacin B. Thus, after the formation of the ion m/z 423, the fragmentation pathways of the linadiacins A and B become identical, resulting in the formation of the ion m/z 381 from both compounds. The formation of this ion (m/z 381) provides evidence of the existence of the malonyl unit in linadiacins A and B (**Table 4**).

Using the positive ionization mode, linadiacins A and B exhibited a particularly abundant fragment ion signal at m/z 365 in their fragment ion spectra (**Table 4**). The ion m/z 365 generated from both linadiacins may correspond to the protonated justicidin B. A high-intensity signal of this ion m/z 365 was also observed in the full MS (MS1) spectra of linadiacins A and B (14.4% and 42.7% relative intensities, **Table 4**) due to the in-source fragmentation of these compounds.

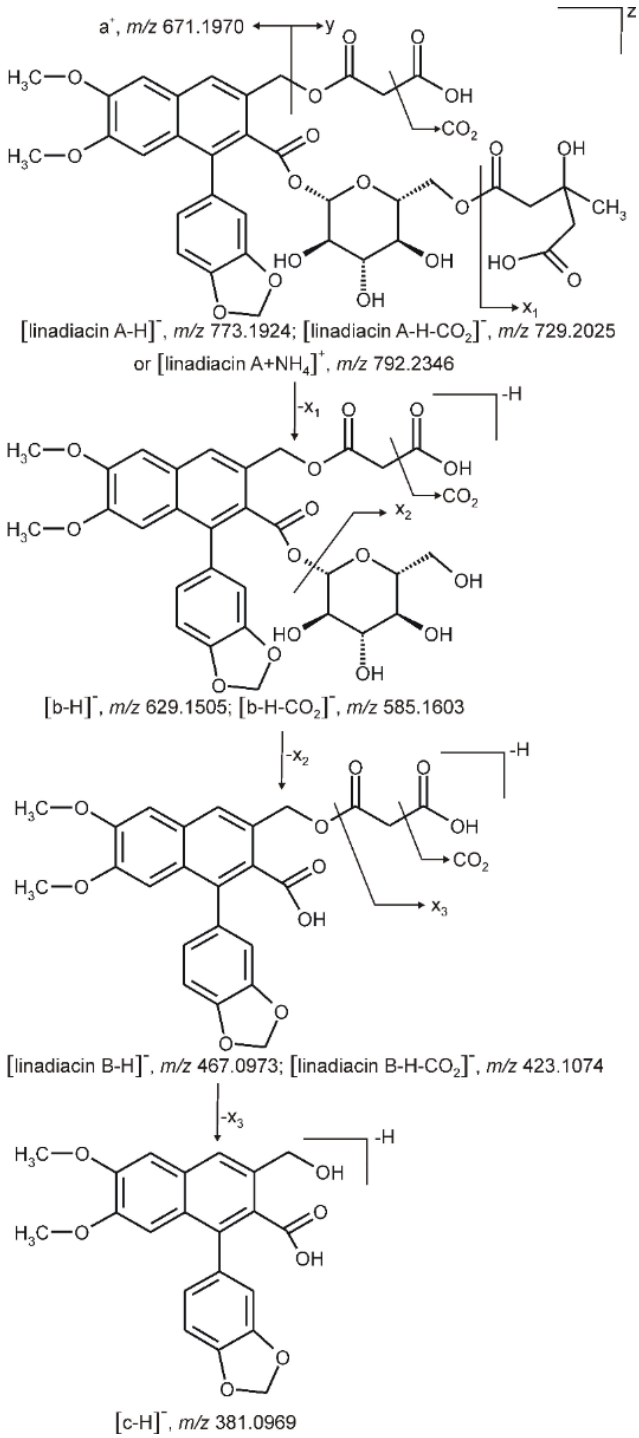

Figure 18. Mass fragmentation route of the deprotonated (**z: -H**) linadiacins A and B analysed by the negative ionization mode, showing the proposed fragment ion structures ([**b-H**]$^-$, **[c-H]**$^-$) and losing moieties (**x**$_1$, **x**$_2$, **x**$_3$). The characteristic fragment ion (**a**$^+$) formed from the ammonium adduct of linadiacin A (**z: +NH**$_4$) after a malonyl loss (**y**), analyzed by the positive ionization mode, is also presented; adapted from author's own work (111).

Even though the Orbitrap Q Exactive Focus mass spectrometer used in this study did not have an MS3 function, the in-source formation of the ion m/z 365 allowed us to study the 2nd generation product ion spectra of linadiacins. The MS2 spectra of the protonated justicidin B and those of the ion m/z 365 formed from linadiacins A and B were highly comparable, containing identical fragment ions. Accordingly, the fragment ion m/z 365 can be identified as justicidin B in the mass spectra of both linadiacins, confirming the identical basic skeleton of linadiacins A and B, which can be converted into justicidin B by hydrolysis and subsequent lactone formation. The mass fragment spectra of linadiacin A (**Table 4**) generated by the positive ionization mode exhibited additional characteristic fragment ions with m/z 671, m/z 653, m/z 635, m/z 617, and m/z 599 that can be explained by the elimination of the malonyl group followed by the successive loss of four H_2O molecules. The H_2O losses confirm the presence of the four free hydroxyl groups of linadiacin A.

5.2.3 *In vitro* SARS-CoV-2 inhibitory activity of arylnaphthalene lignans isolated from *Linum* spp.

Given that the isolated lignans are well tolerated by Vero E6 cells, this cell line represents a suitable host system for the intracellular evaluation of their inhibitory activity against SARS-CoV-2 (**Figure 12**).

Justicidin B was the most effective, followed by diphyllin: both compounds showed a greater than 3-log reduction in viable viruses at a treatment concentration as low as 12.5 μM. Our results are in good accordance with those of a recent study that confirmed a significant anti-SARS-CoV-2 activity (IC_{50} =1.92 μM) and low toxicity (CC_{50} value >100 μM) in the Vero E6 host cells for diphyllin (**Figure 12**) (27).

Literature data further indicate that the antiviral activities of diphyllin mono-, di-, and triglycosides against SARS-CoV-2, tick-borne encephalitis virus (TBEV) (27), and human immunodeficiency virus 1 (HIV-1) are markedly reduced compared to the free aglycone diphyllin, being 3.4-, 6.3-, 13.0-, and 62.1-fold lower, respectively (89). Due to these reports, diphyllin glycosides were not isolated from our *Linum* samples to test their anti-SARS-CoV-2 activity.

5.2.4 Antiproliferative activity of arylnaphthalene lignans isolated from *Linum* spp.

Recently, diphyllin has been reported to exhibit significant antiproliferative activity against human cancer cell lines. In non-small-cell lung cancer A549 cells, IC_{50} values of approximately 2.02 μM and 24.01 μM have been described under different experimental conditions (81,83). In prostate cancer PC-3 cells, diphyllin inhibited cell proliferation with an IC_{50} value of approximately 7.2 μM (82). Our results support the antiproliferative potential of diphyllin against these cells. Furthermore, the remarkable antiproliferative activity of (i) diphyllin against A549, A2058, and PC-3 cells, (ii) justicidin B against A549, A2058, H838, and PC-3 cells, and (iii) linadiacin A against A2058 and PC-3 cells was confirmed for the first time (**Figure 13**).

5.3 Lignans and malonyl-dicaffeoylquinic acids from *Anthriscus* spp.

5.3.1 Identification of aryltetralin and dibenzylbutyrolactone lignans

Among the analyzed *Anthriscus* species, *A. sylvestris* has previously been reported to contain AT- and DBL-type lignans, including the AT-type deoxypodophyllotoxin (**DPT**) and angeloyl podophyllotoxin (**APT**), as well as the DBL-type dimethylmatairesinol (**DiMeMAT**), yatein (**YA**), and anhydropodorhizol (**AHP**) (90,91). Our analyses confirmed the presence of these lignans in various organs of *A. sylvestris* (**Figures 14**, **15**, **19**).

For the first time, the occurrence of lignans was demonstrated in *A. nitida* and *A. caucalis* (**Figures 14**, **15**, **19**). With the exception of **APT**, which was not detected, all lignans previously identified in *A. sylvestris* were also found in *A. nitida*. *A. caucalis* was confirmed as a new source of **DPT**, **AHP**, and **YA**. In addition, the DBL-type lignans desmethylyatein (**DeMeYA**) and kaerophyllin (**KAP**) were identified in *A. nitida*, establishing this species as the first producer of these compounds within the genus *Anthriscus*. Notably, desmethylyatein (**DeMeYA**) has been proposed as a biosynthetic intermediate in the formation of AT-type lignans such as **DPT**; however, to date it has not been reported as an isolated metabolite in *Anthriscus* species (92).

Regarding lignan abundance, high concentrations were detected in root tissues, with *A. sylvestris* roots containing 1.41% **DPT**, 1.32% **AHP**, 0.91% **APT**, and 0.26% **YA**, while *A. nitida* roots accumulated 1.09% **KAP**, 0.25 % **DeMeYA**, and 0.13 %

DiMeMAT. These levels enabled efficient isolation using a one-step preparative HPLC method, identifying roots of both species as particularly suitable lignan sources. Nevertheless, in *A. caucalis*, the highest overall lignan contents were observed in inflorescence tissues (**Figure 19**).

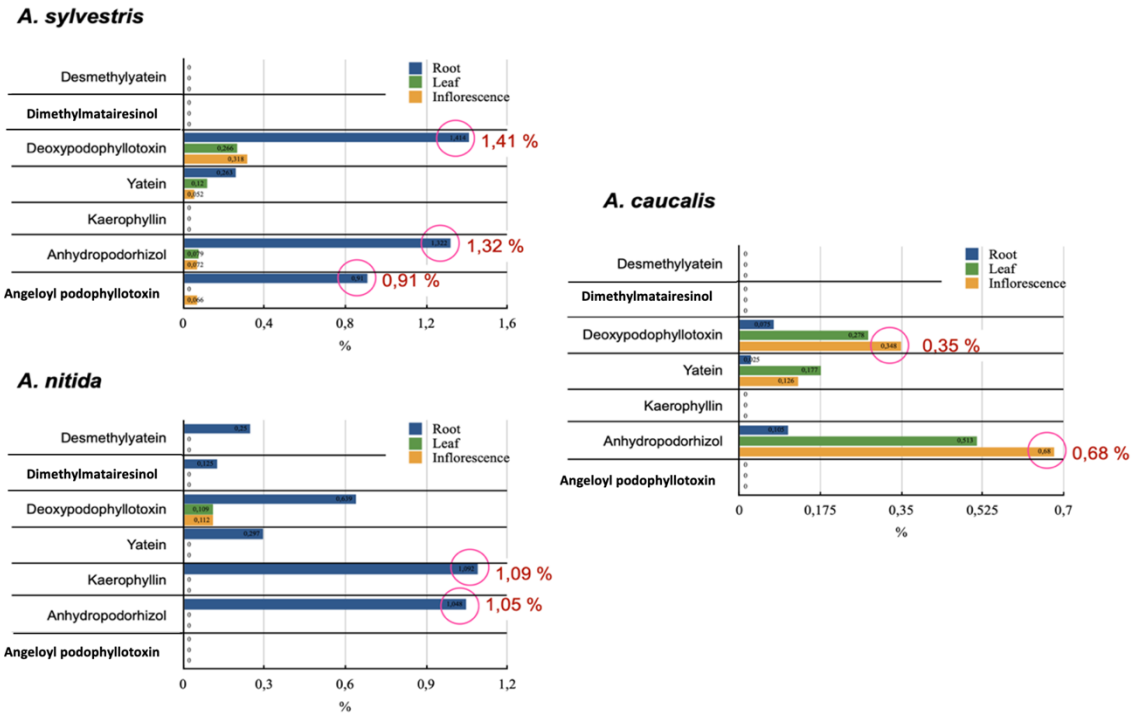

Figure 19. Amounts of lignans (expressed in % of dried tissues) in the root, leaf, and inflorescence tissues of *A. caucalis*, *A. nitida*, and *A. sylvestris* (highest amounts of compounds in the species are marked) (author's own graph based on own data).

5.3.2 Antiproliferative activity of lignans isolated from *A. sylvestris* and *A. nitida*

The isolated AT-type lignans deoxypodophyllotoxin (**DPT**) and angeloyl podophyllotoxin (**APT**), together with the DBL-type lignan anhydropodorhizol (**AHP**), were evaluated for their antiadhesive effects against cancerous HeLa cells and healthy preosteoblast cells by a collaborating research group. Both AT lignans, **DPT** and **APT**, exhibited pronounced antiadhesive activity toward both cell types at submicromolar concentrations, revealing a previously unrecognized mechanism that may contribute to the antiproliferative effects of these natural compounds.

5.3.3 Malonyl-dicaffeoylquinic acids from *A. sylvestris*

High-resolution MS data combined with an extensive NMR study enabled, for the first time, the unambiguous structural elucidation of three MDiCQAs as new natural products: 1,5-dicaffeoyl-3-malonylquinic acid (**HP-1**), 3,5-dicaffeoyl-1-malonylquinic acid (**HP-2**), and 3,5-dicaffeoyl-4-malonyl-epi-quinic acid (**HP-3**) (**Figure 20**). Note: detailed NMR identification of these compounds is in (108).

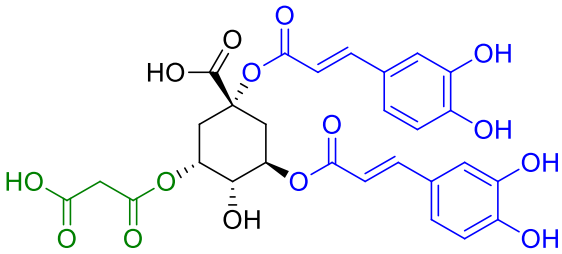

HP-1

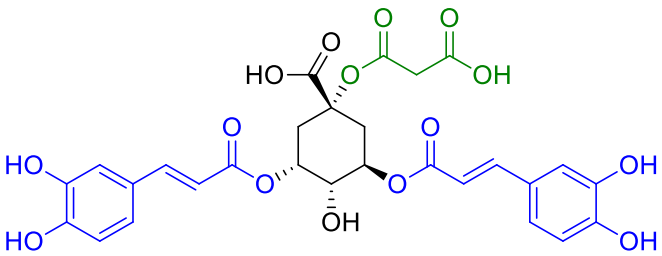

HP-2

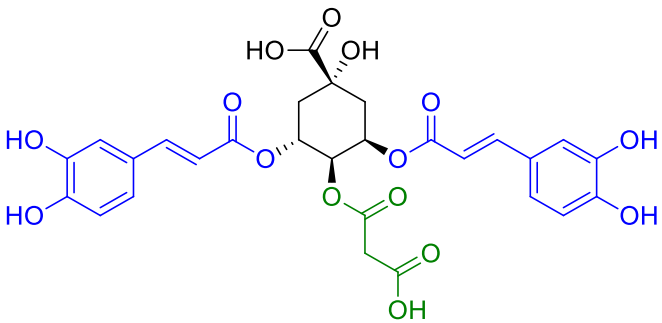

HP-3

Figure 20. Chemical structure of 1,5-dicaffeoyl-3-malonylquinic acid (**HP-1**), 3,5-dicaffeoyl-1-malonylquinic acid (**HP-2**), and 3,5-dicaffeoyl-4-malonyl-epi-quinic acid (**HP-3**), identified as three highly polar compounds from *A. sylvestris*; adapted from own work (113).

The accumulation patterns of these MDiCQAs were clearly organ- and development-phase-dependent. **HP-1** occurred at relatively high levels in all examined tissues, reaching its maximum concentration in inflorescences (**Table 7**). In contrast, **HP-2** and **HP-3** accumulated predominantly in leaves collected at the beginning of the vegetation cycle (**Table 7**). Accordingly, early-spring leaf material represented the most suitable raw material for the simultaneous isolation of all three MDiCQAs.

Among the isolated compounds, **HP-1** was the only MDiCQA to exhibit cytostatic activity, reducing cell viability in several human cancer cell lines. However, **HP-1** also displayed toxicity toward non-tumorigenic Vero E6 cells, indicating a lack of cancer-specific antiproliferative activity (**Table 8**).

6 CONCLUSIONS

This work provides a comprehensive phytochemical and bioactivity-oriented investigation of three plant systems, namely *Forsythia suspensa*, *Linum austriacum* /*L. perenne*, and *Anthriscus* species: focusing on phenylpropanoid-derived metabolites with pharmaceutical relevance. By combining optimized extraction and conversion strategies with advanced chromatographic and spectroscopic techniques, several methodological and biological insights were achieved.

In *Linum* species, detailed conversion studies revealed a previously unknown two-step transformation of a novel arylnaphthalene lignan derivative (linadiacin A) into linadiacin B and ultimately into justicidin B. Acidic and enzymatic treatments enabled selective and quantitative preparation of specific lignans, facilitating their isolation and biological evaluation. The pronounced anti-SARS-CoV-2 activity of diphyllin and justicidin B, combined with their acceptable cytotoxicity profiles, underscores their potential as promising antiviral lead compounds.

In *Anthriscus* species, lignans were identified for the first time in *A. nitida* and *A. caucalis*, expanding the chemotaxonomic knowledge of the genus. Roots of *A. sylvestris* and *A. nitida* were confirmed as rich sources of aryltetralin and dibenzylbutyrolactone lignans, enabling efficient one-step isolation. Furthermore, three malonyl-dicaffeoylquinic acids (MDiCQAs) were structurally elucidated for the first time as new natural products. Their organ- and developmental stage-dependent accumulation patterns were defined, and early-spring leaves were identified as optimal isolation materials. Non-cancer-specific activity was confirmed for the representative of MDiCQAs, contributing to the evaluation of their pharmacological relevance.

In *Forsythia suspensa*, tandem mass spectrometry did not enable discrimination among the isomeric caffeoyl phenylethanoid glycosides (CPhEGs), highlighting the need for complementary analytical approaches for their reliable differentiation.

Overall, this study demonstrates that targeted tissue selection combined with controlled enzymatic and thermal conversion strategies significantly enhances access to bioactive natural products. The integration of these approaches with advanced analytical techniques provides an effective framework for the isolation and evaluation of minor or unstable metabolites, expands chemotaxonomic knowledge, and supports the identification of promising antiviral and antiproliferative lead compounds.

7 SUMMARY

Plant tissues are an important source of pharmacologically relevant natural products, but their accessibility is often limited by low abundance, instability, and tissue-specific distribution. These challenges were addressed through a systematic phytochemical and bioactivity-guided investigation of *Forsythia suspensa*, *Linum austriacum*/*L. perenne*, and *Anthriscus* species, combining advanced analytical methods with controlled conversion strategies to optimize the identification, isolation, and evaluation of phenylpropanoid-derived metabolites.

In *Forsythia suspensa*, isomeric CPhEGs (forsythosides A, H, and I) were identified by mass spectrometry; however, fragmentation analysis confirmed their structural similarity without enabling their discrimination.

In *Linum austriacum* and *L. perenne*, a detailed conversion study of AN lignans revealed the presence of two previously unknown natural compounds, linadiacin A and B. Linadiacin A underwent a quantitative two-step conversion via linadiacin B to justicidin B under acidic conditions. Optimized acidic and enzymatic treatments enabled the selective enrichment and isolation of linadiacins, diphyllin, and justicidin B, with structures and fragmentation pathways confirmed by HR-MS and NMR. Biological evaluation revealed strong *in vitro* anti-SARS-CoV-2 activity of diphyllin and justicidin B at low micromolar concentrations with acceptable cytotoxicity, along with pronounced antiproliferative effects.

In *Anthriscus* species, comprehensive metabolite profiling established *A. nitida* and *A. caucalis* as new natural sources of AT and DBL lignans. Roots of *A. sylvestris* and *A. nitida* were lignan-rich, enabling efficient one-step isolation and identification of desmethylyatein in *A. nitida* provides new insight into lignan biosynthesis. Additionally, three MDiCQAs were structurally elucidated for the first time as new natural products from *A. sylvestris*. Their accumulation was shown to be strongly organ- and development-stage-dependent, with early-spring leaves representing optimal raw materials. Although only one MDiCQA exhibited cytostatic activity, its lack of cancer selectivity underscores the importance of early toxicity screening.

This work integrates tissue selection, controlled conversion processes, and advanced analytical techniques to enable efficient access to minor or unstable metabolites and to support the identification of antiviral and antiproliferative compounds.

8 BIBLIOGRAPHY

1. Xue Z, Yang B. Phenylethanoid glycosides: research advances in their phytochemistry, pharmacological activity and pharmacokinetics. Molecules. 2016;21(8):991.
2. Alcázar Magaña A, Kamimura N, Soumyanath A, Stevens JF, Maier CS. Caffeoylquinic acids: chemistry, biosynthesis, occurrence, analytical challenges, and bioactivity. Plant J. 2021;107(5):1299–319.
3. Umezawa T. Diversity in lignan biosynthesis. Phytochem Rev. 2003;2(3):371–90.
4. Vogt T. Phenylpropanoid biosynthesis. Mol Plant. 2010;3(1):2–20.
5. Jiménez C, Riguera R. Phenylethanoid glycosides in plants: structure and biological activity. Nat Prod Rep. 1994;11(6):591–606.
6. Wink M. Secondary metabolites: their function and evolution. Berlin: Springer; 2010.
7. Heldt H-W, Piechulla B. Plant biochemistry. 4th ed. London: Academic Press; 2010.
8. Fu G, Pang H, Wong YH. Naturally occurring phenylethanoid glycosides: potential leads for new therapeutics. Curr Med Chem. 2008;15(25):2592–613.
9. Teponno RB, Kusari S, Spiteller M. Recent advances in research on lignans and neolignans. Nat Prod Rep. 2016;33(9):1044–92.
10. Liu L, Sun Y, Wen C, Jiang T, Tian W, Xie X, Cui X, Lu R, Feng J, Jin A, Wen S, Wei W. Metabolome analysis of genus *Forsythia*-related constituents in *Forsythia suspensa* leaves and fruits using UPLC-ESI-QQQ-MS/MS technique. PLoS One. 2022;17(6):e0269915.
11. Berežni S, Mimica-Dukić N, Domina G, Raimondo FM, Orčić D. *Anthriscus sylvestris*-noxious weed or sustainable source of bioactive lignans? Plants (Basel). 2024;13(8):1087.
12. Gai F, Janiak MA, Sulewska K, Peiretti PG, Karamać M. Phenolic compound profile and antioxidant capacity of flax (*Linum usitatissimum L.*) harvested at different growth stages. Molecules. 2023;28(4):1807.
13. Kim HJ, Yu YG, Park H, Lee YS. Antiviral lignans from *Forsythia koreana* fruits. Planta Med. 2002;68:1034.

14. Żuk M, Kulma A, Czuj T. Review of pharmacologically active lignans in *Linum* species. Phytochem Rev. 2020;19(5):1223–45.
15. Ikeda R, Nagao T, Okabe H, Nakano Y, Matsunaga H, Katano M, Mori M. Cytotoxic constituents from *Anthriscus sylvestris*. Chem Pharm Bull. 1998;46:871–4.
16. Herrmann KM, Weaver LM. The shikimate pathway. Annu Rev Plant Physiol Plant Mol Biol. 1999;50:473–503.
17. Alipieva K, Korkina L, Orhan IE, Georgiev MI. Verbascoside - a review of its occurrence, (bio)synthesis and pharmacological significance. Biotechnol Adv. 2014;32(6):1065–76.
18. Davin LB, Jourdes M, Patten AM, Kim KW, Vassão DG, Lewis NG. Dissection of lignan biosynthesis in *Linum usitatissimum* (flax) and implications for metabolic engineering. In: Kader JC, Delseny M, editors. Advances in botanical research. Vol. 47. London: Academic Press; 2008. p. 155–207.
19. Shah Z, Gohar UF, Jamshed I, Mushtaq A, Mukhtar H, Zia-UI-Haq M, Toma SI, Manea R, Moga M, Popovici B. Podophyllotoxin: history, recent advances and future prospects. Biomolecules. 2021;11(4):603.
20. Schmidt TJ. Arylnaphthalene lignans – structural diversity, biological activity and prospects for biotechnology. Phytochem Rev. 2012;11(2–3):307–20.
21. Jackson DE, Dewick PM. Aryltetralin lignans from *Podophyllum peltatum* and *Podophyllum hexandrum*. Phytochemistry. 1984;23(5):1147–52.
22. Ishikawa T, Umezawa T. The lignan biosynthetic pathway in *Anthriscus sylvestris*: molecular cloning and characterization of pinoresinol–lariciresinol reductase. Plant Cell Physiol. 2001;42(2):246–53.
23. Bhattacharyya J, Sharma RP. Lignans from *Podophyllum hexandrum*. Phytochemistry. 1975;14(3):827–9.
24. Davin LB, Lewis NG. Dirigent proteins and dirigent sites explain the mystery of specificity of radical precursor coupling in lignan and lignin biosynthesis. Plant Physiol. 2000;123(2):453–62.
25. Pihlaja K, Halonen P, Waissmann W. Lignans from *Chaerophyllum maculatum*. Phytochemistry. 1980;19(2):275–8.

26. Malarz J, Stojakowska A, Kisiel W. Hairy roots as producers of coumarins, lignans, and other phenolic secondary metabolites. Molecules. 2025;30(17):3596.
27. Štefánik M, Bhosale DS, Haviernik J, Straková P, Fojtíková M, Dufková L, Huvarová I, Salát J, Bartáček J, Svoboda J, Sedlák M, Růžek D, Miller AD, Eyer L. Diphyllin shows a broad-spectrum antiviral activity against multiple medically important enveloped RNA and DNA viruses. Viruses. 2022;14(2):354.
28. Nedelcheva R, Zarev Y, Ionkova I. Comparative quantitative profiling of rare justicidin B in *in vitro* cultivated *Linum* species. Pharmacia. 2024;71(1):1–5.
29. Hemmati S, Schneider B, Schmidt TJ, Federolf K, Alfermann AW, Fuss E. Justicidin B 7-hydroxylase, a cytochrome P450 monooxygenase from cell cultures of *Linum perenne* Himmelszelt involved in the biosynthesis of diphyllin. Phytochemistry. 2007;68(22–24):2736–43.
30. Naumenko-Svetlova AA, Akulov AN, Povydysh MN, Zhmud EV, Pozdnyakov DI, Goryacha OV, Kolisnyk SV, Kislichenko VS, Shikov AN. Phenolic compounds in the genus *Linum*. Biomolecules. 2023;13(2):287.
31. Lee KH, Hall IH, Mar EC, Starnes CO, El Gebaly SA, Waddell TG, Hadgraft I. Antitumor agents. 48. Justicidin A and B, new lignans from *Justicia procumbens*. J Med Chem. 1980;23(9):970–3.
32. Ramesh P, Rao PS, Subramanyam M. Diphyllin and related lignans from *Cleistanthus collinus*. Phytochemistry. 1988;27(12):3855–7.
33. Wang Z, Xia Q, Liu X, Liu W, Huang W, Mei X, Luo J, Shan M, Lin R, Zou D, Ma Z. Phytochemistry, pharmacology, quality control and future research of *Forsythia suspensa* (Thunb.) Vahl: A review. J Ethnopharmacol. 2018; 210:318–339.
34. Kitagawa S, Hisada S, Nishibe S. Phenolic compounds from *Forsythia* leaves. Phytochemistry. 1984;23(8):1635–6.
35. Jiao J, Gai QY, Luo M, Wang W, Gu CB, Zhao CJ, Zu YG, Wei FY, Fu YJ. Comparison of main bioactive compounds in tea infusions with different seasonal *Forsythia suspensa* leaves by liquid chromatography–tandem mass

spectrometry and evaluation of antioxidant activity. Food Res Int. 2013;53(2):857–63.

36. Qu H, Li B, Li X, Tu G, Lü J, Sun W. Qualitative and quantitative analyses of three bioactive compounds in different parts of *Forsythia suspensa* by high-performance liquid chromatography-electrospray ionization-mass spectrometry. Microchem J. 2008;89 (2): 159–64.
37. Taskova RM, Gotfredsen CH, Jensen SR. Chemotaxonomic markers in *Digitalideae* (Plantaginaceae). Phytochemistry. 2005;66 (12): 1440–7.
38. Shoyama Y, Matsumoto M, Nishioka I. Four caffeoyl glycosides from callus tissue of *Rehmannia glutinosa*. Phytochemistry. 1986; 25 (7): 1633–6.
39. Di Fabio A, Bruni A, Poli F, Garbarino JA, Chamy MC, Piovano M, Nicoletti M. The distribution of phenylpropanoid glycosides in Chilean *Calceolaria* spp. Biochem Syst Ecol. 1995; 23 (2): 179–82.
40. Kitagawa S, Nishibe S, Benecke R, Thieme H. Phenolic Compounds from *Forsythia* Leaves. II. Chem Pharm Bull, 1988; 36 (9): 3667–70.
41. Qi M, Zhao S, Zhou B, Zhang M, Zhang H, Wang Y, Hu P. Probing the degradation mechanism of forsythiaside A and simultaneous determination of three forsythiasides in *Forsythia* preparations by a single marker. J Sep Sci. 2019; 42 (23): 3503–11.
42. Wang FN, Ma ZQ, Liu Y, Guo YZ, Gu ZW. New phenylethanoid glycosides from the fruits of *Forsythia suspensa* (Thunb.) Vahl. Molecules. 2009;14(4):1324–31.
43. Stojković D, Drakulić D, Schwirtlich M, Rajčević N, Stevanović M, Soković MD, Gašić U. Extract of Herba *Anthrisci cerefolii*: chemical profiling and insights into its anti-glioblastoma and antimicrobial mechanisms of action. Pharmaceuticals (Basel). 2021;14(1):55–70.
44. Deshpande S, Matei MF, Jaiswal R, Bassil BS, Kortz U, Kuhnert N. Synthesis, structure, and tandem mass spectrometric characterization of the diastereomers of quinic acid. J Agric Food Chem. 2016;64(38):7298–306.
45. Ha YH, Kim C, Choi K, Kim JH. Molecular phylogeny and dating of *Forsythieae* (Oleaceae) provide insight into the Miocene history of Eurasian temperate shrubs. Front Plant Sci. 2018;9:99.

46. Deyama T, Kobayashi H, Nishibe S, Tu P. Isolation, structure elucidation and bioactivities of phenylethanoid glycosides from *Cistanche*, *Forsythia* and *Plantago* plants. In: Atta-ur-Rahman, editor. Studies in Natural Products Chemistry. Vol. 33. Amsterdam: Elsevier; 2006. p. 645–74.
47. Nishibe S. The plant origins of herbal medicines and their quality evaluation. Yakugaku Zasshi. 2002;122(6):363–79.
48. Kuo PC, Hung HY, Nian CW, Hwang TL, Cheng JC, Kuo DH, Lee EJ, Tai SH, Wu TS. Chemical constituents and anti-inflammatory principles from the fruits of *Forsythia suspensa*. J Nat Prod. 2017;80(4):1055–64.
49. Kuang HX, Xia YG, Liang J, Yang BY, Wang QH. Lianqiaoxinoside B, a novel caffeoyl phenylethanoid glycoside from *Forsythia suspensa*. Molecules. 2011;16(7):5674–81.
50. Qu H, Zhang Y, Chai X, Sun W. Isoforsythiaside, an antioxidant and antibacterial phenylethanoid glycoside isolated from *Forsythia suspensa*. Bioorg Chem. 2012;40:87–91.
51. Law AHY, Yang CLH, Lau ASY, Chan GCF. Antiviral effect of forsythoside A from *Forsythia suspensa* (Thunb.) Vahl fruit against influenza A virus through reduction of viral M1 protein. J Ethnopharmacol. 2017;209:236–47.
52. Li H, Wu J, Zhang Z, Ma Y, Liao F, Zhang Y, Wu G. Forsythoside A inhibits the avian infectious bronchitis virus in cell culture. Phytother Res. 2011;25(3):338–42.
53. Tutin TG, Heywood VH, Burges NA, Moore DM, Valentine DH, Walters SM, Webb DA, editors. Flora Europaea. Vols. 1–5. Cambridge: Cambridge University Press; 1964–1980.
54. Mohagheghzadeh A, Schmidt TJ, Alfermann AW. Arylnaphthalene lignans from *in vitro* cultures of *Linum austriacum*. J Nat Prod. 2002;65(1):69–71.
55. Eliasson M, Rumpunen K, Rumpunen J, Rydhmer K. Characterization of Swedish accessions of blue flax (*Linum perenne*) for breeding of ornamental cultivars. Sci Hortic (Amsterdam). 2021;288:110354.
56. Jullian-Pawlicki N, Lequart-Pillon M, Huynh-Cong L, Lesur D, Cailleu D, Mesnard F, Laberche JC, Gontier E, Boitel-Conti M. Arylnaphthalene and aryltetralin-type lignans in hairy root cultures of *Linum perenne*, and the

stereochemistry of 6-methoxypodophyllotoxin and one diastereoisomer by HPLC–MS and NMR spectroscopy. Phytochem Anal. 2015;26(5):310–9.

57. Hou W, Huang LJ, Huang H, Liu SL, Dai W, Li ZM, Zhang ZY, Xin SY, Wang JY, Zhang ZY, Ouyang X, Lan JX. Bioactivities and mechanisms of action of diphyllin and its derivatives: a comprehensive systematic review. Molecules. 2023;28(23):7874.
58. Ferraz AC, Gomes PWP, Menegatto MBS, Lima RLS, Guimarães PH, Reis JDE, Carvalho ARV, Pamplona SGSR, Muribeca AJB, Magalhães JCM, Silva CYY, Silva MN, Magalhães CLB. Exploring the antiviral potential of justicidin B and four glycosylated lignans from *Phyllanthus brasiliensis* against Zika virus. Phytomedicine. 2024;123:155197.
59. Vasilev N, Ionkova I. Production of justicidin B, a cytotoxic arylnaphthalene lignan from genetically transformed root cultures of *Linum leonii*. J Nat Prod. 2006;69(7):1014–7.
60. Momekov G, Konstantinov S, Dineva I, Ionkova I. Effect of justicidin B—a potent cytotoxic and pro-apoptotic arylnaphthalene lignan—on human breast cancer-derived cell lines. Neoplasma. 2011;58(4):320–5.
61. Sciandrone B, Kentsop RAD, Pensotti R, Ottolina G, Mascheretti I, Mattana M. Toxicological analysis of the arylnaphthalene lignan justicidin B. Molecules. 2024;29(23):5516.
62. Tang YQ, Pan XH, Shang FF, Li Y, Zhang CJ, Ma HX, Zhang ZQ, Wu SJ, Zhou XB, Ma ZL. Synthesis and pharmacological evaluation of natural-product diphyllin derivatives against head and neck squamous cell carcinoma. Eur J Med Chem. 2025;285:117215.
63. Ren J, Zhang L, Wang X, Cui W, Wang L, Li J, Zhao Y. Biological activities and therapeutic potential of diphyllin and its derivatives. Phytother Res. 2025;39(4):1632–48.
64. Spalik K. Revision of *Anthriscus* (Apiaceae). Pol Bot Stud. 1997;13:1–69.
65. Tekin M, Civelek Ş. A taxonomic revision of the genus *Anthriscus* (Apiaceae) in Turkey. Phytotaxa. 2017;302(1):1–26.
66. Kurzyna-Młynik R, Kosiński P, Chudzińska E, Surina B, Konowalik KE, Wojewódzka A, Spalik K. Phylogeographic evidence reveals multiple

colonization events and a secondary contact zone in the Balkans for the *Anthriscus sylvestris* complex. Sci Rep. 2025;15:15409.

67. Olaru OT, Venables L, van de Venter M, Nitulescu GM, Margina D, Spandidos DA, Tsatsakis AM. Ethnomedicinal, phytochemical and pharmacological profile of *Anthriscus sylvestris* as an alternative source for anticancer lignans. Molecules. 2015;20(6):10037–54.
68. Shah Z, Gohar UF, Jamshed I, Mushtaq A, Mukhtar H, Zia-ul-Haq M, Nabavi SM, Kaselis V. Phytochemical and pharmacological advances on *Anthriscus sylvestris* and related species. Biomolecules. 2021;11(4):603.
69. Golakoti T, Kancharla HK, Meka B, Murthy YLN. Phytochemical characterization and antioxidant potential of *Anthriscus* extracts. Med Chem Res. 2016;25:2906–15.
70. Miranda-Vera C, Hernández ÁP, García-García P, Díez D, García PÁ, Castro MÁ. Metabolomic analysis of *Anthriscus sylvestris* inflorescences reveals phenolic diversity with potential pharmacological relevance. Pharmaceutics. 2023;15:2728.
71. Strus P, Sadowski K, Ploch W, Gunia-Krzyżak A, Wójcik-Pszczoła K, Maruszewicz H, Popiół J. Anti-inflammatory and antioxidant effects of *Anthriscus sylvestris* flower extracts in human dermal models. Int J Mol Sci. 2025;26:958.
72. Berežni S, Mimica-Dukić N, Domina G, Raimondo FM. *Anthriscus sylvestris*—noxious weed or sustainable source of bioactive lignans? Plants (Basel). 2024;13(8):1087.
73. Orčić D, Francišković M, Božin B, Mimica-Dukić N, Berežni S, Igić R, Štefánik M. Comprehensive study of *Anthriscus sylvestris* lignans. Phytochemistry. 2021;190:112883.
74. Orčić D, Francišković M, Božin B, Mimica-Dukić N, Berežni S, Igić R, Štefánik M. Quantitative HPLC–UV study of lignans in *Anthriscus sylvestris*. Molecules. 2022;27(18):6072.
75. Olaru OT, Nitulescu GM, Orțan A, Dinu-Pîrvu CE. Ethnomedicinal, phytochemical and pharmacological profile of *Anthriscus sylvestris* as an alternative source for anticancer lignans. Molecules. 2015;20(8):15004–28.

76. Swor K, Satyal P, Setzer WN. The essential oil composition of *Anthriscus caucalis* M. Bieb. (Apiaceae) growing wild in southwestern Idaho. Nat Prod Commun. 2023;18(8):1934578X231187699.
77. Bedows E. Antiviral activity of lignans. J Nat Prod. 1998;61(5):686–702.
78. Medarde M, Jiménez A, Caballero E, Gordaliza M, del Corral JMM, San Felix A, Khalid SA. Lignans from *Juniperus sabina* L. and their cytotoxic and antiviral activity. Planta Med. 1995;61(6):511–4.
79. Saleem M, Kim HJ, Ali MS, Lee YS. An update on bioactive lignans. Nat Prod Rep. 2005;22(6):696–716.
80. Byler KG, Ogungbe IV, Setzer WN. *In silico* screening for anti-Zika virus phytochemicals. J Mol Graph Model. 2016;69:78–91.
81. Wang YR, Xu Y, Jiang ZZ, Guerram M, Wang B, Zhu X, Zhang YL, Han ZZ, Yuan ZH, Zhang LY. Deoxypodophyllotoxin induces G2/M cell-cycle arrest and apoptosis in SGC-7901 cells and inhibits tumor growth *in vivo*. Molecules. 2015;20(1):1661–75.
82. Hu S, Zhou Q, Wu WR, Duan YX, Gao ZY, Li YW, Xu YB. Anticancer effect of deoxypodophyllotoxin induces apoptosis of human prostate cancer cells. Oncol Lett. 2016;12(5):2918–23.
83. Yang Y, Liu L, Sun J, Wang S, Yang Z, Li H, Jiang Z. Deoxypodophyllotoxin inhibits non-small-cell lung cancer cell growth by reducing HIF-1α-mediated glycolysis. Front Oncol. 2021;11:629543.
84. Chen Q, Liu W, Ma H, He X, Zhang Y, Zhao Y, Zhang YM. Deoxypodophyllotoxin induces apoptosis and autophagy in human hepatocellular carcinoma cells through ROS-mediated PI3K/Akt/mTOR signaling. Chem Biol Interact. 2020;324:109090.
85. Lee YJ, Lim YJ, Yoon H, Kim JH, Kim BH, Kim Y. Yatein induces G2/M cell-cycle arrest and apoptosis through microtubule destabilization in human lung carcinoma cells. Biochem Pharmacol. 2019;163:26–36.
86. Bhattacharyya J, Sharma RP. Lignans from *Podophyllum hexandrum* and *Anthriscus sylvestris*. Phytochemistry. 1975;14(3):827–9.

87. Hendrawati O, Woerdenbag HJ, Michiels PJA, Aantjes HG, van Dam A, Kayser O. Identification of lignans and related compounds in *Anthriscus sylvestris* by LC-ESI-MS/MS and LC-SPE-NMR. Phytochemistry. 2011;72(16):2172–83.
88. Jia J, Zhang F, Li Z, Qin X, Zhang L. Comparison of fruits of *Forsythia suspensa* at two different maturation stages by NMR-based metabolomics. Molecules. 2015;20(6):10065–81.
89. Chang RS, Yeung HW. Inhibition of growth of human immunodeficiency virus *in vitro* by crude extracts of Chinese medicinal herbs. Antiviral Res. 1988;9:163–75.
90. Seegers A, Kiss AK. Comparison of extraction methods for lignans from *Anthriscus sylvestris* Hoffm. Planta Med. 2017;83(6):507–14.
91. Koulman A, Batterman S, van Uden W, Pras N. Lignan production in cell cultures of *Anthriscus sylvestris*. Planta Med. 2003;69(7):635–40.
92. Sakakibara N, Suzuki S, Umezawa T, Shimada M. Biosynthesis of yatein in *Anthriscus sylvestris*. Org Biomol Chem. 2003;1(14):2474–85.
93. Könye R, Tóth G, Sólyomváry A, Mervai Z, Zürn M, Baghy K, Kovalszky I, Horváth P, Molnár-Perl I, Noszál B, Béni S, Boldizsár I. Chemodiversity of *Cirsium* fruits: Antiproliferative lignans, neolignans and sesquineolignans as chemotaxonomic markers. Fitoterapia. 2018;127:413–9.
94. Sólyomváry A, Mervai Z, Tóth G, Ress ÁE, Noszál B, Molnár-Perl I, Baghy K, Kovalszky I, Boldizsár I. A simple and effective enrichment process of the antiproliferative lignan arctigenin based on the endogenous enzymatic hydrolysis of *Serratula tinctoria* and *Arctium lappa* fruits. Process Biochem. 2015;50(12):2281–8.
95. McDill J, Repplinger M, Simpson BB, Kadereit JW. Phylogeny of *Linum* and evolution of heterostyly based on nuclear and chloroplast sequence data. Syst Bot. 2009;34(2):386–405.
96. Medarde M, Peláez-Lamamié de Clairac R, López JL, Grávalos DG, San Feliciano A. Synthesis, antitumoral and antiviral evaluation of halo- and demethyl-yatein derivatives. Arch Pharm (Weinheim). 1995;328(9):640–4.
97. Suthiwong J, Wandee J, Pitchuanchom S, Sojikul P, Kukongviriyapan V, Yenjai C. Cytotoxicity against cholangiocarcinoma and HepG2 cell lines of

lignan derivatives from *Hernandia nymphaeifolia*. Med Chem Res. 2018;27:2214–23.

98. Kwak YS, Lee DH, Kim HJ, Kim JH, Yim NH, Yoo HS, Kim JS. Deoxypodophyllotoxin, a lignan from *Anthriscus sylvestris*, induces apoptosis and cell cycle arrest by inhibiting the EGFR signaling pathways in esophageal squamous cell carcinoma cells. Int J Mol Sci. 2020;21(18):6854.
99. Kusari S, Kusari P, Spiteller M, Kayser O. *Aspergillus fumigatus Fresenius*, an endophytic fungus from *Juniperus communis* L. Horstmann as a novel source of the anticancer pro-drug deoxypodophyllotoxin. J Appl Microbiol. 2009;107(3):1019–30.
100. Loike JD, Brewer CF, Sternlicht H, Gensler WJ, Horwitz SB. Structure–activity study of the inhibition of microtubule assembly *in vitro* by podophyllotoxin and its congeners. Cancer Res. 1978;38(9):2688–93.
101. Sudo K, Konno K, Shigeta S, Yokota T. Inhibitory effects of podophyllotoxin derivatives on herpes simplex virus replication. Antiviral Chem Chemother. 1998;9(3):263–7.
102. Gordaliza M, Castro A, del Corral JMM, San Feliciano A, García-Grávalos MD. Antineoplastic and antiviral activities of podophyllotoxin-related lignans. Arch Pharm (Weinheim). 1994;327:175–9.
103. Lee SH, Son MJ, Ju HK, Lin CX, Moon TC, Choi HG, Son JK, Chang HW. Dual inhibition of cyclooxygenases-2 and 5-lipoxygenase by deoxypodophyllotoxin in mouse bone marrow-derived mast cells. Biol Pharm Bull. 2004;27(5):786–8.
104. Dall'Acqua S, Giorgetti M, Cervellati R, Innocenti G. Deoxypodophyllotoxin content and antioxidant activity of aerial parts of *Anthriscus sylvestris* Hoffm. Z Naturforsch C J Biosci. 2006;61(9–10):658–62.
105. Jeong GS, Kwon OK, Park BY, Oh SR, Ahn KS, Chang MJ, Oh WK, Kim JC, Min BS, Kim YC, Lee HK. Lignans and coumarins from the roots of *Anthriscus sylvestris* and their increase of caspase-3 activity in HL-60 cells. Biol Pharm Bull. 2007;30(7):1340–3.
106. Donoso-Fierro C, Cuellar M, Muñoz M, Alarcón J, Speisky H, Céspedes CL. Antiproliferative activity of yatein isolated from *Austrocedrus chilensis*

against murine myeloma cells: cytological studies and chemical investigations. Pharm Biol. 2015;53(3):378–85.

107. Golakoti T, Kancharla HK, Meka BYLN, Murthy B. Efficient synthesis of lactonic and thionolactonic lignans and evaluation of their antioxidant, anti-inflammatory and cytotoxic activities. Med Chem Res. 2016;25:2906–15.

108. Nazli A. Dissertation, Budapest: Semmelweis University; in preparation.

109. Zürn M. Phytochemical investigation of phenylethanoid glycosides and lignans in selected species of the *Oleaceae* and *Plantaginaceae* families [dissertation]. Budapest: Semmelweis University; 2023.

110. Zürn M, Tóth G, Ausbüttel T, Mucsi Z, Horváti K, Bősze S, Pályi B, Kis Z, Noszál B, Boldizsár I. Tissue-specific accumulation and isomerization of valuable phenylethanoid glycosides from *Plantago* and *Forsythia* plants. Int J Mol Sci. 2021;22(8):3880.

111. Tóth G, Horváti K, Kraszni M, Ausbüttel T, Pályi B, Kis Z, Mucsi Z, Kovács GM, Bősze S, Boldizsár I. Arylnaphthalene lignans with anti-SARS-CoV-2 and antiproliferative activities from the underground organs of *Linum austriacum* and *Linum perenne*. J Nat Prod. 2023;86(8):1375–87.

112. Péter B[1], Ausbüttel T[1], Kanyo N, Joó P, Tóth K, Szittner Z, Szekacs I, Bősze S, Kovács GM, Boldizsár I, Horvath R. *In situ* monitoring of cell adhesion kinetics using label-free optical biosensors: Evaluating anticancer potential and selectivity of natural compounds. VIEW. 2025;6(1):20240043.

113. Nazli A, Gáborová M, Ausbüttel T, Stipsicz B, Tóth G, Bősze S, Béni S, Boldizsár I. Malonyl-caffeoylquinic acids and malonyl-flavonoid-glucosides from three edible Apiaceae plants *Anthriscus cerefolium*, *Anthriscus sylvestris*, and *Chaerophyllum bulbosum*. ACS Omega. 2025;10(1):235.

9 BIBLIOGRAPHY OF CANDIDATE'S PUBLICATIONS

9.1 Publications related to the thesis

1. Péter B[1], **Ausbüttel T[1]**, Kanyo N, Joó P, Tóth K, Szittner Z, Szekacs I, Bősze S, Kovács GM, Boldizsár I, Horvath R. *In situ* monitoring of cell adhesion kinetics using label-free optical biosensors: Evaluating anticancer potential and selectivity of natural compounds. **VIEW**. **2025**;6(1):20240043.

2. Nazli A, Gáborová M, **Ausbüttel T**, Stipsicz B, Tóth G, Bősze S, Béni S, Boldizsár I. Malonyl-caffeoylquinic acids and malonyl-flavonoid-glucosides from three edible Apiaceae plants *Anthriscus cerefolium*, *Anthriscus sylvestris*, and *Chaerophyllum bulbosum*. **ACS Omega**. **2025**;10(1):235.

3. Tóth G, Horváti K, Kraszni M, **Ausbüttel T**, Pályi B, Kis Z, Mucsi Z, Kovács GM, Bősze S, Boldizsár I. Arylnaphthalene lignans with anti-SARS-CoV-2 and antiproliferative activities from the underground organs of *Linum austriacum* and *Linum perenne*. **J Nat Prod**. **2023**;86(8):1375–87.

4. Zürn M, Tóth G, **Ausbüttel T**, Mucsi Z, Horváti K, Bősze S, Pályi B, Kis Z, Noszál B, Boldizsár I. Tissue-specific accumulation and isomerization of valuable phenylethanoid glycosides from *Plantago* and *Forsythia* plants. **Int J Mol Sci**. **2021**;22(8):3880.

10 ACKNOWLEDGEMENT

First of all, I would like to express my sincere and deepest gratitude to my supervisor, **Dr. Imre Boldizsár**, for his excellent guidance and support throughout my PhD research. I am truly grateful to have had the opportunity to be mentored by such an outstanding researcher.

I would also like to thank **Dr. Ágnes Alberti-Dér**, Director of the Department of Pharmacognosy at Semmelweis University, for providing me with the opportunity to pursue my PhD studies.

I am particularly grateful to **Dr. Gábor Kovács**, Head of the Department of Plant Anatomy at Eötvös Loránd University (ELTE), for granting access to the department's facilities, where the majority of the experiments, including the LC-MS analyses, were carried out.

I am also grateful to **Dr. Szabolcs Béni**, **Dr. Márta Kraszni**, **Dr. Gergő Tóth**, and **Dr. Szilvia Bősze** for the contributions of performing and evaluating the NMR and *in vitro* analyses.

Finally, I would like to express my deepest gratitude to my **Family** and my girlfriend **Anna** for their constant support and encouragement throughout this journey. I am equally thankful to my my friends **Vera**, **Moritz**, and **Ildi**, whose support and companionship made this experience truly meaningful.